Differential involvement of LUBAC - mediated linear ubiquitination in intestinal epithelial cells and macrophages during intestinal inflammation

AUTHOR(S):

Sakamoto, Yusuke; Sasaki, Katsuhiro; Omatsu, Mayuki; Hamada, Kensuke; Nakanishi, Yuki; Itatani, Yoshiro; Kawada, Kenji; Obama, Kazutaka; Seno, Hiroshi; Iwai, Kazuhiro

CITATION:

Sakamoto, Yusuke ...[et al]. Differential involvement of LUBAC - mediated linear ubiquitination in intestinal epithelial cells and macrophages during intestinal inflammation. The Journal of Pathology 2023, 259(3): 304-317

ISSUE DATE:

2023-03

URL:

http://hdl.handle.net/2433/279249

Article manuscript (Main text 3,989 words)

Title

Differential involvement of LUBAC-mediated linear ubiquitination in intestinal epithelial cells and macrophages during intestinal inflammation

Running title (68 characters)

Linear ubiquitination in intestinal epithelial cells and macrophages

Authors and affiliations

Yusuke Sakamoto[1,2], Katsuhiro Sasaki[1], Mayuki Omatsu[3], Kensuke Hamada[3], Yuki Nakanishi[3], Yoshiro Itatani[2], Kenji Kawada[2], Kazutaka Obama[2], Hiroshi Seno[3] and Kazuhiro Iwai[1]*

[1]Department of Molecular and Cellular Physiology, Graduate School of Medicine, Kyoto University, Kyoto, Japan.

[2]Department of Surgery, Graduate School of Medicine, Kyoto University, Kyoto, Japan.

[3]Department of Gastroenterology and Hepatology, Graduate School of Medicine, Kyoto University, Kyoto, Japan.

***Correspondence to**

Kazuhiro Iwai

Department of Molecular and Cellular Physiology, Graduate School of Medicine, Kyoto University, Yoshida-Konoe-cho, Sakyo-ku, Kyoto 606-8501, Japan

Phone: +81-75-753-4671; Fax: +81-75-753-4676

E-mail: kiwai@mcp.med.kyoto-u.ac.jp

Conflict of interest statement

The authors declare no competing financial interests.

Abstract (284 words)

Disruption of the intestinal epithelial barrier and dysregulation of macrophages are major factors contributing to the pathogenesis of inflammatory bowel diseases (IBDs). Activation of NF-κB and cell death are involved in maintaining intestinal homeostasis in a cell type-dependent manner. Although both are regulated by linear ubiquitin chain assembly complex (LUBAC)-mediated linear ubiquitination, the physiological relevance of linear ubiquitination to intestinal inflammation remains unexplored. Here, we used two experimental mouse models of IBD (intraperitoneal LPS and oral dextran sodium sulphate (DSS) administration) to examine the role of linear ubiquitination in intestinal epithelial cells (IECs) and macrophages during intestinal inflammation. We did this by deleting the linear ubiquitination activity of LUBAC specifically from IECs or macrophages. Upon LPS administration, loss of ligase activity in IECs induced mucosal inflammation and augmented IEC death. LPS-mediated death of LUBAC-defective IECs was triggered by TNF. IEC death was rescued by an anti-TNF antibody, and TNF (but not LPS) induced apoptosis of organoids derived from LUBAC-defective IECs. However, augmented TNF-mediated IEC death did not overtly affect the severity of colitis after DSS administration. By contrast, defective LUBAC ligase activity in macrophages ameliorated DSS-induced colitis by attenuating both infiltration of macrophages and expression of inflammatory cytokines. Decreased production of macrophage chemoattractant MCP-1/CCL2, as well as pro-inflammatory IL-6 and TNF, occurred through impaired activation of NF-κB and ERK via loss of ligase activity in macrophages. Taken together, these results indicate that both intraperitoneal LPS and oral DSS administrations are beneficial for evaluating epithelial integrity under inflammatory conditions, as well as macrophage functions in the event of an epithelial barrier breach. The data clarify the cell-specific roles of linear ubiquitination as a critical regulator of TNF-mediated

epithelial integrity and macrophage pro-inflammatory responses during intestinal inflammation.

Keywords (10)

LUBAC; linear ubiquitination; NF-κB; cell death; intestinal epithelial cells; macrophages; DSS; LPS; IBD; intestinal inflammation

Introduction

Inflammatory bowel diseases (IBDs), including Crohn's disease and ulcerative colitis, are characterized by chronic and relapsing inflammation in the gut; these conditions affect 6.8 million individuals worldwide [1]. Although the pathogenesis of IBDs is thought to involve genetic, environmental, microbial, epithelial, and immune factors, the pathophysiology still remains unclear, resulting in inadequate responses to currently available treatments [2-4]. Recent studies show that the innate immune system, including epithelial barrier function and microbial sensing by macrophages, also plays an important role in the pathogenesis of IBDs, as do adaptive immune responses such as T cell-derived inflammatory cytokines [5-7].

Intestinal epithelial cells (IECs) maintain intestinal homeostasis by forming a physical and chemical barrier that protects intestinal tissue from invading intraluminal bacteria [8-10]. IEC death disrupts intestinal homeostasis in some mouse models [11-18], and excessive IEC death is observed in patients with IBDs [19, 20]. In addition, macrophages, major components of the innate immune system that reside just beneath IECs, play crucial roles as the first line of defense [21-24]. When intestinal homeostasis is perturbed by genetic or environmental factors such as epithelial barrier disruption or macrophage dysregulation, a large number of TLR-expressing pro-inflammatory macrophages migrate into the inflamed mucosa and release pro-inflammatory cytokines and chemokines such as IL-6, TNF, and MCP-1/CCL2 [22–24] in response to products derived from invading bacteria [25]. Although appropriate responses confer protection against bacteria and promote tissue regeneration by acting on other immune cells and IECs, uncontrolled responses lead to persistent inflammation, which inhibits tissue repair [22-24, 26-28].

The linear ubiquitin chain assembly complex (LUBAC), comprising HOIP, HOIL-1L, and SHARPIN, activates the NF-κB signaling pathway and inhibits programmed cell death by generating unique N-terminal-linked linear polyubiquitin chains via the catalytic center in

HOIP [29-32]. Several reports suggest that NF-κB activation maintains IEC homeostasis by inhibiting IEC death; however, activation of NF-κB in macrophages plays a pro-inflammatory role [33-36]. Recent genome-wide association studies also show that NF-κB is associated with IBDs [37]. Despite the essential roles played by NF-κB and cell death during intestinal inflammation, involvement of LUBAC-mediated linear ubiquitination is unclear.

Considering the cell type-specific roles of both NF-κB and cell death [33, 38], we used mice lacking the C-terminal catalytic center of HOIP specifically in IECs ($HOIP^{IEC\text{-}\Delta lin}$) or macrophages ($HOIP^{MYE\text{-}\Delta lin}$) to examine the role of linear ubiquitination in IECs and macrophages. Since no spontaneous intestinal phenotype was observed in either mouse model, we used mouse models of IBD generated by intraperitoneal administration of LPS or by oral administration of dextran sodium sulphate (DSS) [39, 40]. Loss of ligase activity in IECs provoked mucosal inflammation and augmented TNF-mediated IEC death upon LPS administration, indicating that linear ubiquitination in IECs protects against intestinal inflammation and suppresses TNF-induced IEC death under inflammatory conditions. By contrast, loss of LUBAC ligase activity in macrophages alleviated DSS-induced colitis and impaired NF-κB- and ERK-mediated inflammatory cytokine production upon TLR stimulation, indicating that linear ubiquitination in macrophages augments intestinal inflammation in the event of an epithelial barrier breach. These findings demonstrate that linear ubiquitination in IECs and macrophages plays differential roles to maintain both TNF-mediated epithelial integrity and macrophage pro-inflammatory responses to regulate intestinal inflammation.

Materials and methods

Mice

HOIP$^{\Delta lin\text{-}flox/\Delta lin\text{-}flox}$ mice, in which the C-terminal catalytic center of HOIP (*Rnf31*) is flanked by two *loxP* sites, have been described previously [41, 42]. HOIP$^{\Delta lin\text{-}flox/\Delta lin\text{-}flox}$ mice were crossed with *Villin-Cre* [43] or *LysM-Cre* [44] mice to ablate the ligase activity of HOIP in IECs or macrophages, respectively. Unless specified otherwise, mice (aged 8 to 12 weeks) were cohoused with sex-matched littermates under specific pathogen-free conditions. All animal protocols were approved by Kyoto University.

Antibodies

The antibodies used in this study are listed in Supplementary materials and methods.

LPS and TNF-induced IEC death

Mice were injected intraperitoneally with LPS (10 μg/g bodyweight (BW), Escherichia coli 055:B5; Sigma-Aldrich, St. Louis, MO, USA) or recombinant mouse TNF-α (0.1 μg/g BW; R&D Systems, Minneapolis, MN, USA).

TNF depletion experiments

Mice were injected intraperitoneally with an anti-TNF-α antibody (200 μg, clone XT3.11; Bio X Cell, Lebanon, NH, USA) or an isotype control IgG (200 μg, clone TNP6A7; Bio X Cell) 1 h before LPS challenge.

Induction of colitis

Experimental colitis was induced by oral administration of 2.0% or 1.5% DSS (MP Biomedicals, Irvine, CA, USA) dissolved in drinking water (ingested for 7 or 5 days), followed by of normal

water (ingested for 2 or 5 days).

Histological analysis

The distal third of the colon or ileal segment was fixed in 10% formalin and embedded in paraffin. The severity of DSS-induced colitis was determined by examining H&E-stained sections, as described previously [45]. Multiple viewing fields per slide were acquired randomly under an Olympus BX51 upright microscope (Olympus, Tokyo, Japan) or a FLUOVIEW FV1000 confocal laser scanning microscope (Olympus).

IEC isolation and organoid culture

IEC isolation and generation of organoids were performed as previously described [46]. To examine cell death, cells were stained with 5 μM SYTOX Green nucleic acid stain (Invitrogen, Waltham, MA, USA) and 5 μg/ml Hoechst 33342 nucleic acid stain (Invitrogen), which were added to the medium, followed by observation under an IX83 Inverted Research Microscope (Olympus). Organoids were treated with LPS (Sigma-Aldrich) or TNF-α (R&D Systems). Z-VAD-FMK (ZVAD) (PEPTIDE, Osaka, Japan) was added 1 h before TNF treatment.

Enrichment of bone marrow-derived macrophages

Bone marrow-derived macrophages (BMDMs) were isolated from bone marrow from the tibia and femur and cultured for 7 days in complete RPMI containing 20 ng/ml recombinant murine M-CSF (BioLegend, San Diego, CA, USA). BMDMs were stimulated with TNF, LPS, Poly(I:C) (InvivoGen, San Diego, CA, USA), CpG-B (InvivoGen), or Pam3CSK4 (InvivoGen). For some experiments, HOIPin-8 (Axon Medchem LLC, Reston, VA, USA) or a MEK inhibitor (PD0325901; FUJIFILM, Osaka, Japan) was added before stimulation.

155 Statistical analysis

156 Results are expressed as the mean ± SEM. Statistical analyses were performed using

157 GraphPad Prism Version9.3.1 (GraphPad Software, San Diego, CA, USA). All statistical tests

158 are indicated in each figure legend. The significance level was set at $P < 0.05$.

159

Results

Mice lacking linear ubiquitination activity in IECs display mucosal inflammation and augmented IEC death upon intraperitoneal administration of LPS

To investigate the role of LUBAC-mediated linear ubiquitination in IECs, we crossed HOIP$^{\Delta lin\text{-}flox/\Delta lin\text{-}flox}$ mice [41, 42] with *Villin-Cre* mice [43] to delete the linear ubiquitination activity of LUBAC (HOIP Δlinear) specifically in IECs (HOIP$^{IEC\text{-}\Delta lin}$ mice) (supplementary material, Figure S1A). Immunoblotting revealed that *Cre*-mediated recombination of HOIP loci (*Rnf31*), as evaluated by the decrease in full-length HOIP, was not complete (expression of full-length HOIP in the colon and the small intestine of HOIP$^{IEC\text{-}\Delta lin}$ mice was 49.2 ± 2.1% and 28.8 ± 3.7%, respectively, of that observed in control HOIP$^{\Delta lin\text{-}flox/\Delta lin\text{-}flox}$ mice; supplementary material, Figure S1B). This was also the case for organoid cultures (31.5 ± 5.4% expression in HOIP$^{IEC\text{-}\Delta lin}$ organoids compared with control organoids; supplementary material, Figure S1B). The amounts of HOIL-1L and SHARPIN, the other two subunits of LUBAC, were also reduced (supplementary material, Figure S1B). HOIP$^{IEC\text{-}\Delta lin}$ mice developed normally (supplementary material, Figure S1C); however, whole-body deletion of HOIP was embryonic lethal [47, 48]. There were no overt changes in tissue architecture, nor defects in IEC differentiation, in the colon or small intestine under steady-state conditions (supplementary material, Figure S1D–F).

Intraperitoneal administration of LPS causes shedding of IECs in the small intestine [39, 49]. LUBAC-mediated linear ubiquitination plays a role in protecting cells from programmed cell death [30, 32, 50, 51]. We found that HOIP$^{IEC\text{-}\Delta lin}$ mice were extremely sensitive to intraperitoneal administration of LPS; these mice showed a significant reduction in colon length, and marked mucosal damage in the distal colon, at 24 h post-LPS treatment (Figure 1A, B). Immunohistological analysis revealed increased infiltration of the distal colon by leukocytes, including macrophages (Figure 1C, D and supplementary material, Figure S2). Moreover, at 4 h post-LPS administration the number of apoptotic cells that were cleaved

caspase 3- and TUNEL-positive was higher in the distal colon of HOIP $^{IEC\text{-}\Delta lin}$ mice than in that of control mice, although there was no difference in the number of apoptotic cells under steady-state conditions (Figure 1E, F). In particular, apoptotic cells were detected in all layers of the distal colon, including the crypt bottom, in HOIP$^{IEC\text{-}\Delta lin}$ mice (Figure 1E, F). The inflammatory changes in the distal colon in HOIP$^{IEC\text{-}\Delta lin}$ mice were not observed in the small intestine (supplementary material, Figure S3A). However, apoptotic cells were detected in the crypts and villous tips in HOIP$^{IEC\text{-}\Delta lin}$ small intestine at 1.5 h post-LPS administration, along with an increase in the number of apoptotic IECs; however, apoptotic cells were observed only at the villous tips in the small intestine of control mice, regardless of LPS administration (supplementary material, Figure S3B, C) [39, 52]. Taken together, these data suggest that loss of LUBAC ligase activity in IECs renders mice more sensitive to IEC death in the colon and small intestine after intraperitoneal injection of LPS, which may lead to mucosal inflammation (although no inflammatory changes were observed in the small intestine).

TNF drives LPS-induced mucosal inflammation and augmented IEC death in mice lacking epithelial LUBAC ligase activity

To examine the mechanism underlying IEC death in LPS-treated HOIP$^{IEC\text{-}\Delta lin}$ mice, we established intestinal epithelial organoids. There were no morphological differences between HOIP$^{IEC\text{-}\Delta lin}$ and control organoids, and LPS-treatments induced no apparent morphological changes in the organoids (Figure 2A). Because shedding of IECs is thought to be triggered by inflammatory cytokines produced by LPS-stimulated macrophages [39, 49], and LUBAC-mediated linear ubiquitination protects cells from TNF-induced cell death (including apoptosis and necroptosis) [30, 32, 50, 51], we focused on TNF as LPS administration induced expression of TNF in the serum and colon tissues of HOIP$^{IEC\text{-}\Delta lin}$ and control mice (Figure 2B, C). We found that HOIP$^{IEC\text{-}\Delta lin}$ organoids exhibited a disrupted and

dark appearance as early as 24 h after TNF treatment (Figure 2A). After treatment with TNF, the proportion of SYTOX Green-positive organoids was higher for HOIP$^{IEC\text{-}\Delta lin}$ than for controls, indicating that TNF, but not LPS, is responsible for cell death in HOIP$^{IEC\text{-}\Delta lin}$ organoids (Figure 2A). Immunoblotting revealed that cleavage of both caspase 8 and 3 was higher in TNF-treated HOIP$^{IEC\text{-}\Delta lin}$ organoids, whereas phosphorylation of MLKL, an executor of necroptosis, was not detected in either HOIP$^{IEC\text{-}\Delta lin}$ or control organoids (Figure 2D). These data suggest that TNF preferentially triggers apoptosis of HOIP$^{IEC\text{-}\Delta lin}$ organoids. In addition, degradation of IκBα, a hallmark of NF-κB activation, was impaired substantially in HOIP$^{IEC\text{-}\Delta lin}$ organoids upon TNF stimulation (Figure 2E), and expression of NF-κB target genes, including anti-apoptotic genes, was partially attenuated in HOIP$^{IEC\text{-}\Delta lin}$ organoids exposed to TNF (Figure 2F). These results indicate that loss of LUBAC ligase activity sensitizes organoids to TNF-induced apoptosis (at least in part) by impairing NF-κB activation.

Intraperitoneal injections of TNF provoked mucosal inflammation in the colon of HOIP$^{IEC\text{-}\Delta lin}$ mice, with shortening of the colon and increased invasion by inflammatory cells; this was not observed in control mice (Figure 3A–D and supplementary material, Figure S2). Immunohistochemical analysis revealed increased numbers of cleaved caspase 3-positive IECs in the colon of HOIP$^{IEC\text{-}\Delta lin}$ mice (Figure 3E). Although H&E staining revealed that changes in the small intestine of HOIP$^{IEC\text{-}\Delta lin}$ mice were less pronounced than those in the colon (supplementary material, Figure S3D), cleaved caspase 3-positive apoptotic cells in the small intestine of TNF-treated HOIP$^{IEC\text{-}\Delta lin}$ mice were observed at the crypt bottom and the villous tips (supplementary material, Figure S3E, F). Pretreatment with the anti-TNF antibody prevented LPS-induced inflammatory changes in HOIP$^{IEC\text{-}\Delta lin}$ mice, including shortening of the colon, infiltration of the colon by immune cells and apoptosis of IECs (Figure 3F-J and supplementary material, Figure S3G–I). Collectively, these results indicate that LUBAC-

induced linear ubiquitination protects mice from LPS-induced mucosal inflammation and TNF-induced IEC death.

Defective LUBAC catalytic activity in macrophages, but not in IECs, ameliorates DSS-induced colitis

To examine whether IEC death in HOIP$^{IEC\text{-}\Delta lin}$ mice has an effect on the phenotype of another mouse model of IBD, we fed HOIP$^{IEC\text{-}\Delta lin}$ and control mice with 2% or 1.5% DSS, a direct chemical toxin to IECs [53], for 7 or 5 days. However, loss of the LUBAC ligase activity in IECs did not overtly affect severity of DSS-induced colitis (including BW changes, shortening of the colon, histological changes, or expression of inflammatory cytokines) (Figure 4A–D and supplementary material, Figure S4). In addition, we examined apoptotic IECs in DSS-treated HOIP$^{IEC\text{-}\Delta lin}$ mice, and observed cleaved caspase 3- and TUNEL-positive IECs in some crypts that escaped DSS-induced direct injury (Figure 4E). Thus, we suspect that loss of linear ubiquitination activity in IECs does not overtly affect the severity of DSS-induced colitis, despite the tendency toward increased IEC death; this may be because DSS damages IECs directly.

Next, we examined the role played by linear ubiquitination in macrophages during intestinal inflammation because macrophages represent the first line of defense after epithelial barrier disruption [24]. To this end, we crossed HOIP$^{\Delta lin\text{-}flox/\Delta lin\text{-}flox}$ mice with *LysM-Cre* mice [44] to generate mice lacking the catalytic center of HOIP specifically in macrophages (HOIP$^{MYE\text{-}\Delta lin}$). We observed a marked reduction (44.2 ± 0.7%) in expression of full-length HOIP, along with HOIL-1L and SHARPIN, in HOIP$^{MYE\text{-}\Delta lin}$ BMDMs compared with control BMDMs (supplementary material, Figure S5A, B). This was also the case for peritoneal macrophages, in which expression of full-length HOIP in HOIP$^{MYE\text{-}\Delta lin}$ mice was attenuated significantly, albeit not completely (supplementary material, Figure S5A). HOIP$^{MYE\text{-}\Delta lin}$ mice

developed normally, and no inflammatory or autoimmune phenotypes were observed in the intestine or the skin of aged HOIP$^{MYE\text{-}\Delta lin}$ mice (supplementary material, Figure S5C, D). Additionally, there was no abnormality in the proportions of activated lymphocytes, including germinal center B cells (PNA^{+}FAS^{+}), activated T cells (CD25^{+}CD69^{+}), or effector T cells (CD44^{hi}CD62L^{lo}), in the spleen or peripheral lymph nodes of aged HOIP$^{MYE\text{-}\Delta lin}$ mice (supplementary material, Figure S6).

To evaluate involvement of linear ubiquitination in macrophages after an epithelial barrier breach, we fed HOIP$^{MYE\text{-}\Delta lin}$ and control mice with DSS. We found that inflammatory changes, including weight loss and shortening of the colon, were less severe in HOIP$^{MYE\text{-}\Delta lin}$ mice than in control mice (Figure 5A, B). Histological analysis revealed that mucosal damage in the distal colon was less severe in HOIP$^{MYE\text{-}\Delta lin}$ mice than in control mice (Figure 5C). Immunohistological analysis also showed that the number of the leukocytes, including macrophages, B cells, and T cells, was lower in DSS-treated HOIP$^{MYE\text{-}\Delta lin}$ mice (Figure 5D, E and supplementary material, Figure S7). Moreover, expression of inflammatory cytokines in the colon was significantly lower (Figure 5F). Next, we injected HOIP$^{MYE\text{-}\Delta lin}$ and control mice intraperitoneally with LPS, because macrophages are thought to be involved in the pathogenesis of the LPS-induced IEC shedding [39]. However, regardless of LUBAC ligase activity, we found no overt differences in the number of apoptotic IECs in the small intestine, or the levels of inflammatory cytokines in serum or intestinal tissue (supplementary material, Figure S8). Collectively, the data suggest that attenuated linear ubiquitination in macrophages ameliorates the severity of colitis after an epithelial breach induced by DSS.

Attenuation of LUBAC ligase activity in macrophages impairs NF-κB- and ERK-mediated production of inflammatory cytokines in response to TLR stimulation

283 To address the molecular mechanisms underlying amelioration of DSS-induced
284 colitis in HOIP$^{MYE-\Delta lin}$ mice, we stimulated BMDMs from HOIP$^{MYE-\Delta lin}$ and control mice with
285 TNF [30-32]. We found that phosphorylation and degradation of IκBα, as well as
286 phosphorylation of p65 and IKK, were lower in TNF-stimulated HOIP$^{MYE-\Delta lin}$ BMDMs than in
287 control BMDMs (Figure 6A). Studies suggest that TLRs expressed by pro-inflammatory
288 macrophages play a role in DSS-induced colitis [22, 23]. Upon LPS stimulation, not only
289 phosphorylation and degradation of IκBα, but also phosphorylation of IKK and p65, was
290 impaired in HOIP$^{MYE-\Delta lin}$ BMDMs (Figure 6B), indicating that loss of LUBAC ligase activity
291 in macrophages attenuates LPS-mediated activation of NF-κB. IKK activation in macrophages
292 leads to activation of ERK [42, 54, 55]; here, we found that LPS-induced phosphorylation of
293 ERK was lower in HOIP$^{MYE-\Delta lin}$ BMDMs than in control BMDMs (Figure 6C). By contrast,
294 loss of LUBAC ligase activity did not overtly affect activation of other MAPK pathways,
295 including p38 and JNK (Figure 6C). To confirm the role of LUBAC-mediated linear
296 ubiquitination during LPS signaling in macrophages, we treated BMDMs from WT mice with
297 HOIPin-8, a specific inhibitor of LUBAC ligase activity [56]. As shown in Figure 6D, LPS-
298 mediated activation of NF-κB and ERK was attenuated markedly by HOIPin-8, whereas
299 activation of JNK and p38 was not. These results indicate that linear ubiquitination is involved
300 in LPS-triggered activation of NF-κB and ERK, but not p38 or JNK, in macrophages.
301 Augmented cell death is observed in some cells with attenuated LUBAC activity [30, 32, 50,
302 51]. However, linear ubiquitination in macrophages has no obvious effect on TNF-mediated
303 cell death, regardless of the presence of cycloheximide, or LPS-induced cell death in HOIP^{MYE-}
304 $^{\Delta lin}$ BMDMs, or DSS-treated HOIP$^{MYE-\Delta lin}$ mice (supplementary material, Figure S9).

305 Next, we asked how loss of linear ubiquitination affects inflammatory cytokine
306 production upon TLR stimulation. LPS-induced production of IL-6, TNF, and MCP-1/CCL2
307 (a chemoattractant for macrophages) fell significantly in HOIP$^{MYE-\Delta lin}$ BMDMs and HOIPin-8-

treated BMDMs from WT mice (Figure 6E, F). Because treatment with a MEK inhibitor suppressed TNF and MCP-1/CCL2 (Figure 6G), we speculated that ERK acts synergistically with NF-κB to trigger production of inflammatory cytokines. Lastly, we investigated LUBAC involvement in other TLR signaling pathways. Upon stimulation with TLR ligands Poly(I:C), CpG-B, or Pam3CSK4, phosphorylation and degradation of IκBα, and phosphorylation of IKK and p65, was substantially attenuated by pretreatment with HOIPin-8 (supplementary material, Figure S10). ERK activation was impaired markedly by HOIPin-8 downstream of these ligands (supplementary material, Figure S10). Furthermore, production of IL-6 by HOIP$^{\text{MYE-}\Delta\text{lin}}$ BMDMs was impaired substantially in response to Poly(I:C), CpG-B, and Pam3CSK4 (Figure 6H), suggesting that linear ubiquitination is involved in signaling via multiple TLRs. Collectively, these results suggest that linear ubiquitination in macrophages augments intestinal inflammation in the event of an epithelial barrier breach induced by DSS, possibly due to increased production of pro-inflammatory cytokines and a macrophage chemoattractant downstream of NF-κB and ERK pathway activation by multiple TLR ligands.

Discussion

Dysfunction of the epithelial barrier and unrestrained inflammatory responses by macrophages are major factors contributing to the pathogenesis of IBDs [22-24, 57]. Since cell-specific targeting is vital to uncover the roles of NF-κB- and cell death-related pathways [33, 38], we examined the role of LUBAC ligase activity, which controls NF-κB activation and programmed cell death [29-32], in both IECs and macrophages during intestinal inflammation. To do this, we used two experimental mouse models of IBD. Loss of the LUBAC ligase activity in IECs or macrophages resulted in different phenotypes: IEC-specific loss of linear ubiquitination activity sensitized mice to mucosal inflammation after LPS administration, whereas loss of activity in macrophages ameliorated DSS-induced colitis.

Mice with IEC-specific deletion of molecules essential for NF-κB activation or protection from TNF-mediated cell death exhibit spontaneous severe intestinal inflammation due to the augmented sensitivity to TNF-induced cell death [11, 14]. However, HOIP$^{IEC\text{-}\Delta lin}$ mice did not develop spontaneous histological abnormalities in the intestines (supplementary material, Figure S1D–F), despite the crucial role of LUBAC-mediated linear ubiquitination in NF-κB activation and protection from cell death [32, 50, 51]. Observations in the intestines of HOIP$^{IEC\text{-}\Delta lin}$ mice were in sharp contrast to those in skin (another border between the environment and the body), in which attenuated LUBAC function triggers spontaneous dermatitis due to TNF-mediated cell death [50, 58, 59]. The mechanisms responsible for the discrepancy between the skin and intestine are unknown; however, the finding that LUBAC ligase activity in IECs is dispensable for intestinal homeostasis enabled us to evaluate two IBD models: LPS-mediated IEC shedding and DSS-induced colitis [39, 40]. Loss of the LUBAC ligase activity in IECs rendered mice susceptible to mucosal inflammation and augmented IEC death upon intraperitoneal injection of LPS (Figure 1); this was phenocopied by TNF injection (Figure 3A–E), and was rescued by an anti-TNF antibody (Figure 3F–J). We also found that TNF induced

apoptosis of HOIP$^{IEC\text{-}\Delta lin}$ organoids; however, LPS did not (Figure 2A, D), which was due in part to the compromised NF-κB pathway (Figure 2E, F). At present, we do not know why we could not detect inflammation in the small intestine of LPS-treated HOIP$^{IEC\text{-}\Delta lin}$ mice, despite augmented epithelial apoptosis (supplementary material, Figure S3A–C). However, mechanisms other than NF-κB- or LUBAC-mediated pathways may act to maintain integrity of the small intestine. TNF is involved in the pathogenesis of IBDs in humans because TNF-targeted therapy is a highly effective treatment [60], and TNF is also a potent driver of epithelial barrier disruption [11, 14, 17, 20, 61]. Our results clearly highlight a crucial role for LUBAC-mediated linear ubiquitination in maintaining TNF-induced epithelial integrity under inflammatory conditions (supplementary material, Figure S11).

In contrast to the LPS-induced IEC shedding model, HOIP$^{IEC\text{-}\Delta lin}$ mice did not exhibit obvious sensitivity to DSS-induced colitis (Figure 4A–D). In this model, mice receive oral DSS for several days; however, in the LPS-induced IEC shedding model, IEC shedding is usually evaluated within 1 day of LPS administration [15, 39, 40, 49]. We found that HOIP$^{IEC\text{-}\Delta lin}$ mice displayed mucosal inflammation within 24 h of LPS administration (Figure 1). Moreover, it is suspected that administration of DSS, a direct chemical toxin to IECs, for several days leads to massive disruption of IECs [53], which might suggest that augmented sensitivity to intestinal inflammation and IEC death in HOIP$^{IEC\text{-}\Delta lin}$ mice cannot be properly evaluated by DSS administration. Therefore, the DSS-induced colitis model alone may not be suitable for probing the mechanism underlying disruption of epithelial integrity within a short time. An LPS-induced IEC shedding model together with DSS-induced colitis model might be more beneficial for evaluating the pathogenesis of IBDs.

Pro-inflammatory macrophages accumulate and respond in a highly pro-inflammatory manner to stimulation of TLR ligands after epithelial disruption induced by DSS [22, 23]. In contrast to HOIP$^{IEC\text{-}\Delta lin}$ mice (Figure 4), HOIP$^{MYE\text{-}\Delta lin}$ mice displayed attenuated mucosal damage and

less infiltration by immune cells, as well as induction of inflammatory cytokines, upon DSS-induced epithelial injury (Figure 5). We observed that loss of the LUBAC ligase activity in BMDMs stimulated with LPS led to decreased production of macrophage chemoattractant MCP-1/CCL2, as well as pro-inflammatory IL-6 and TNF, downstream of attenuated NF-κB and ERK activation (Figure 6). Since loss of the LUBAC ligase activity did not overtly augment macrophage death (supplementary material, Figure S9), downregulated expression of MCP-1/CCL2 (Figure 5F and 6E, F), not induction of cell death, is likely responsible for decreased accumulation of macrophages (Figure 5D, E), which might further attenuate inflammatory responses in DSS-treated HOIP$^{MYE\text{-}\Delta lin}$ mice. Collectively, the data suggest that linear ubiquitination in macrophages augments intestinal inflammation in the event of an epithelial barrier breach by promoting recruitment of macrophages to sites of damage, as well as by up-regulating production of pro-inflammatory cytokines via activation of the NF-κB and ERK pathways (supplementary material, Figure S11).

By contrast, IEC shedding upon intraperitoneal injection of LPS was comparable in HOIP$^{MYE\text{-}\Delta lin}$ and control mice (supplementary material, Figure S8A). This might be because there is no overt difference in expression of inflammatory cytokines between LPS-treated HOIP$^{MYE\text{-}\Delta lin}$ and control mice (supplementary material, Figure S8B, C). We suspected that dendritic cells, effector T cells, adipocytes, and fibroblasts (in addition to macrophages) might produce IL-6 and TNF upon LPS injection because these cells produce these cytokines as a direct or indirect response to LPS [26, 27]. Macrophages play pleiotropic roles during acute inflammation, including activation of other immune cells, elimination of infectious agents, and promotion of tissue regeneration, whereas prolonged inflammation delays tissue repair [22-24, 26-28]. Thus, loss of LUBAC ligase activity in macrophages may prevent prolonged inflammation and facilitate epithelial repair in DSS-induced colitis (Figure 5) without affecting acute inflammatory responses that are necessary for tissue regeneration.

In conclusion, we show here that linear ubiquitination in IECs and macrophages plays a role in the pathogenesis of IBDs. While direct epithelial injury by DSS administration is useful for investigate macrophage function as the first line of defense in the innate immune system, rapid and indirect IEC shedding induced by LPS administration might also be a suitable option for investigating the mechanisms that maintain epithelial integrity. Linear ubiquitination in IECs and macrophages functions differentially during intestinal inflammation by regulating TNF-mediated epithelial integrity and macrophage pro-inflammatory responses, respectively; therefore, cell-specific targeting of linear ubiquitination might be a novel approach to treating IBDs.

Acknowledgments

We thank the Center for Anatomical, Pathological and Forensic Medical Research, Kyoto University Graduate School of Medicine, for preparing tissue sections. We also thank Drs. S. Kuno, Y. Shinkawa, Y. Fuseya, T. Jo, Y. Takeda, I. Yanatori, H. Fujita, and M. Kim for insightful discussion and advice, and Ms Y. Akasaki, Y. Hayamizu, and N. Ueno for technical assistance. This work was supported by JSPS KAKENHI Grant Numbers 17H06174 and 18H05499 (to K. I.).

Author contributions

Y. S., Y. N., K. S., and K. I. conceived and designed the study. Y. S. performed the experiments. M. O. and K. H. supported organoid culture. Y. I., K. K., K. O., and H. S. provided crucial advice. Y. S. and K. I. wrote the manuscript, with contributions from all other authors.

References

1. Collaborators GBDIBD. The global, regional, and national burden of inflammatory bowel disease in 195 countries and territories, 1990-2017: a systematic analysis for the Global Burden of Disease Study 2017. *Lancet Gastroenterol Hepatol* 2020; **5:** 17-30.

2. Sartor RB. Mechanisms of disease: pathogenesis of Crohn's disease and ulcerative colitis. *Nat Clin Pract Gastroenterol Hepatol* 2006; **3:** 390-407.

3. de Souza HS, Fiocchi C. Immunopathogenesis of IBD: current state of the art. *Nat Rev Gastroenterol Hepatol* 2016; **13:** 13-27.

4. Chang JT. Pathophysiology of Inflammatory Bowel Diseases. *N Engl J Med* 2020; **383:** 2652-2664.

5. Geremia A, Biancheri P, Allan P, *et al.* Innate and adaptive immunity in inflammatory bowel disease. *Autoimmun Rev* 2014; **13:** 3-10.

6. Schey R, Danzer C, Mattner J. Perturbations of mucosal homeostasis through interactions of intestinal microbes with myeloid cells. *Immunobiology* 2015; **220:** 227-235.

7. Baillie JK, Arner E, Daub C, *et al.* Analysis of the human monocyte-derived macrophage transcriptome and response to lipopolysaccharide provides new insights into genetic aetiology of inflammatory bowel disease. *PLoS Genet* 2017; **13:** e1006641.

8. Artis D. Epithelial-cell recognition of commensal bacteria and maintenance of immune homeostasis in the gut. *Nat Rev Immunol* 2008; **8:** 411-420.

9. Turner JR. Intestinal mucosal barrier function in health and disease. *Nat Rev Immunol* 2009; **9:** 799-809.

10. Peterson LW, Artis D. Intestinal epithelial cells: regulators of barrier function and immune homeostasis. *Nat Rev Immunol* 2014; **14:** 141-153.

11. Nenci A, Becker C, Wullaert A, *et al.* Epithelial NEMO links innate immunity to chronic intestinal inflammation. *Nature* 2007; **446:** 557-561.

12. Welz PS, Wullaert A, Vlantis K, *et al.* FADD prevents RIP3-mediated epithelial cell necrosis and chronic intestinal inflammation. *Nature* 2011; **477:** 330-334.

13. Dannappel M, Vlantis K, Kumari S, *et al.* RIPK1 maintains epithelial homeostasis by inhibiting apoptosis and necroptosis. *Nature* 2014; **513:** 90-94.

14. Takahashi N, Vereecke L, Bertrand MJ, *et al.* RIPK1 ensures intestinal homeostasis by protecting the epithelium against apoptosis. *Nature* 2014; **513:** 95-99.

15. Gunther C, Buchen B, He GW, *et al.* Caspase-8 controls the gut response to microbial challenges by Tnf-α-dependent and independent pathways. *Gut* 2015; **64:** 601-610.

16. Eftychi C, Schwarzer R, Vlantis K, *et al.* Temporally Distinct Functions of the Cytokines IL-12 and IL-23 Drive Chronic Colon Inflammation in Response to Intestinal Barrier Impairment. *Immunity* 2019; **51:** 367-380 e364.

17. Schwarzer R, Jiao H, Wachsmuth L, *et al.* FADD and Caspase-8 Regulate Gut Homeostasis and Inflammation by Controlling MLKL- and GSDMD-Mediated Death of Intestinal Epithelial Cells. *Immunity* 2020; **52:** 978-993 e976.

18. Nakanishi Y, Reina-Campos M, Nakanishi N, *et al.* Control of Paneth Cell Fate, Intestinal Inflammation, and Tumorigenesis by PKCλ/ι. *Cell Rep* 2016; **16:** 3297-3310.

19. Iwamoto M, Koji T, Makiyama K, *et al.* Apoptosis of crypt epithelial cells in ulcerative colitis. *J Pathol* 1996; **180:** 152-159.

20. Gunther C, Martini E, Wittkopf N, *et al.* Caspase-8 regulates TNF-α-induced epithelial necroptosis and terminal ileitis. *Nature* 2011; **477:** 335-339.

21. Smith PD, Smythies LE, Shen R, *et al.* Intestinal macrophages and response to microbial encroachment. *Mucosal Immunol* 2011; **4:** 31-42.

22. Bain CC, Mowat AM. Macrophages in intestinal homeostasis and inflammation. *Immunol Rev* 2014; **260:** 102-117.

23. Bain CC, Schridde A. Origin, Differentiation, and Function of Intestinal

469 Macrophages. *Front Immunol* 2018; **9:** 2733.

470 24. Na YR, Stakenborg M, Seok SH*, et al.* Macrophages in intestinal inflammation and

471 resolution: a potential therapeutic target in IBD. *Nat Rev Gastroenterol Hepatol* 2019; **16:**

472 531-543.

473 25. Akira S, Uematsu S, Takeuchi O. Pathogen recognition and innate immunity. *Cell*

474 2006; **124:** 783-801.

475 26. Friedrich M, Pohin M, Powrie F. Cytokine Networks in the Pathophysiology of

476 Inflammatory Bowel Disease. *Immunity* 2019; **50:** 992-1006.

477 27. Neurath MF. Cytokines in inflammatory bowel disease. *Nat Rev Immunol* 2014; **14:**

478 329-342.

479 28. Karin M, Clevers H. Reparative inflammation takes charge of tissue regeneration.

480 *Nature* 2016; **529:** 307-315.

481 29. Kirisako T, Kamei K, Murata S*, et al.* A ubiquitin ligase complex assembles linear

482 polyubiquitin chains. *EMBO J* 2006; **25:** 4877-4887.

483 30. Tokunaga F, Sakata S, Saeki Y*, et al.* Involvement of linear polyubiquitylation of

484 NEMO in NF-κB activation. *Nat Cell Biol* 2009; **11:** 123-132.

485 31. Iwai K, Tokunaga F. Linear polyubiquitination: a new regulator of NF-κB

486 activation. *EMBO Rep* 2009; **10:** 706-713.

487 32. Ikeda F, Deribe YL, Skanland SS*, et al.* SHARPIN forms a linear ubiquitin ligase

488 complex regulating NF-κB activity and apoptosis. *Nature* 2011; **471:** 637-641.

489 33. Greten FR, Eckmann L, Greten TF*, et al.* IKKβ links inflammation and

490 tumorigenesis in a mouse model of colitis-associated cancer. *Cell* 2004; **118:** 285-296.

491 34. Atreya I, Atreya R, Neurath MF. NF-κB in inflammatory bowel disease. *J Intern*

492 *Med* 2008; **263:** 591-596.

493 35. Pasparakis M. Regulation of tissue homeostasis by NF-κB signalling: implications

for inflammatory diseases. *Nat Rev Immunol* 2009; **9:** 778-788.

36. Liu T, Zhang L, Joo D, *et al.* NF-κB signaling in inflammation. *Signal Transduct Target Ther* 2017; **2**.

37. Jostins L, Ripke S, Weersma RK, *et al.* Host-microbe interactions have shaped the genetic architecture of inflammatory bowel disease. *Nature* 2012; **491:** 119-124.

38. Vereecke L, Vieira-Silva S, Billiet T, *et al.* A20 controls intestinal homeostasis through cell-specific activities. *Nat Commun* 2014; **5:** 5103.

39. Williams JM, Duckworth CA, Watson AJ, *et al.* A mouse model of pathological small intestinal epithelial cell apoptosis and shedding induced by systemic administration of lipopolysaccharide. *Dis Model Mech* 2013; **6:** 1388-1399.

40. Chassaing B, Aitken JD, Malleshappa M, *et al.* Dextran sulfate sodium (DSS)-induced colitis in mice. *Curr Protoc Immunol* 2014; **104:** 15 25 11-15 25 14.

41. Sasaki Y, Iwai K. Crucial Role of Linear Ubiquitin Chain Assembly Complex-Mediated Inhibition of Programmed Cell Death in TLR4-Mediated B Cell Responses and B1b Cell Development. *J Immunol* 2018; **200:** 3438-3449.

42. Sasaki Y, Sano S, Nakahara M, *et al.* Defective immune responses in mice lacking LUBAC-mediated linear ubiquitination in B cells. *EMBO J* 2013; **32:** 2463-2476.

43. el Marjou F, Janssen KP, Chang BH, *et al.* Tissue-specific and inducible Cre-mediated recombination in the gut epithelium. *Genesis* 2004; **39:** 186-193.

44. Clausen BE, Burkhardt C, Reith W, *et al.* Conditional gene targeting in macrophages and granulocytes using LysMcre mice. *Transgenic Res* 1999; **8:** 265-277.

45. Nakatsuji M, Minami M, Seno H, *et al.* EP4 Receptor-Associated Protein in Macrophages Ameliorates Colitis and Colitis-Associated Tumorigenesis. *PLoS Genet* 2015; **11:** e1005542.

46. Sato T, Vries RG, Snippert HJ, *et al.* Single Lgr5 stem cells build crypt-villus

519 structures in vitro without a mesenchymal niche. *Nature* 2009; **459:** 262-265.

520 47. Peltzer N, Rieser E, Taraborrelli L*, et al.* HOIP deficiency causes embryonic

521 lethality by aberrant TNFR1-mediated endothelial cell death. *Cell Rep* 2014; **9:** 153-165.

522 48. Peltzer N, Darding M, Montinaro A*, et al.* LUBAC is essential for embryogenesis

523 by preventing cell death and enabling haematopoiesis. *Nature* 2018; **557:** 112-117.

524 49. Jones LG, Vaida A, Thompson LM*, et al.* NF-κB2 signalling in enteroids modulates

525 enterocyte responses to secreted factors from bone marrow-derived dendritic cells. *Cell Death*

526 *Dis* 2019; **10:** 896.

527 50. Taraborrelli L, Peltzer N, Montinaro A*, et al.* LUBAC prevents lethal dermatitis by

528 inhibiting cell death induced by TNF, TRAIL and CD95L. *Nat Commun* 2018; **9:** 3910.

529 51. Tang Y, Joo D, Liu G*, et al.* Linear ubiquitination of cFLIP induced by LUBAC

530 contributes to TNFα-induced apoptosis. *J Biol Chem* 2018; **293:** 20062-20072.

531 52. Watson AJ, Hughes KR. TNF-α-induced intestinal epithelial cell shedding:

532 implications for intestinal barrier function. *Ann N Y Acad Sci* 2012; **1258:** 1-8.

533 53. Eichele DD, Kharbanda KK. Dextran sodium sulfate colitis murine model: An

534 indispensable tool for advancing our understanding of inflammatory bowel diseases

535 pathogenesis. *World J Gastroenterol* 2017; **23:** 6016-6029.

536 54. Gantke T, Sriskantharajah S, Sadowski M*, et al.* IκB kinase regulation of the TPL-

537 2/ERK MAPK pathway. *Immunol Rev* 2012; **246:** 168-182.

538 55. Webb LV, Ventura S, Ley SC. ABIN-2, of the TPL-2 Signaling Complex, Modulates

539 Mammalian Inflammation. *Trends Immunol* 2019; **40:** 799-808.

540 56. Oikawa D, Sato Y, Ohtake F*, et al.* Molecular bases for HOIPINs-mediated

541 inhibition of LUBAC and innate immune responses. *Commun Biol* 2020; **3:** 163.

542 57. Vereecke L, Beyaert R, van Loo G. Enterocyte death and intestinal barrier

543 maintenance in homeostasis and disease. *Trends Mol Med* 2011; **17:** 584-593.

58. Kumari S, Redouane Y, Lopez-Mosqueda J, *et al.* Sharpin prevents skin inflammation by inhibiting TNFR1-induced keratinocyte apoptosis. *Elife* 2014; **3**.

59. Rickard JA, Anderton H, Etemadi N, *et al.* TNFR1-dependent cell death drives inflammation in Sharpin-deficient mice. *Elife* 2014; **3**.

60. Neurath MF. Current and emerging therapeutic targets for IBD. *Nat Rev Gastroenterol Hepatol* 2017; **14:** 269-278.

61. Pott J, Kabat AM, Maloy KJ. Intestinal Epithelial Cell Autophagy Is Required to Protect against TNF-Induced Apoptosis during Chronic Colitis in Mice. *Cell Host Microbe* 2018; **23:** 191-202 e194.

Figure legends

Figure 1. Deletion of epithelial linear ubiquitination activity sensitizes mice to mucosal inflammation and IEC death upon intraperitoneal administration of LPS.

(A) Representative pictures (left) and quantification of colon length (right) in control and HOIP$^{IEC\text{-}\Delta lin}$ mice at the indicated times post-LPS treatment (n=3–5). ns, not significant.

(B) H&E staining of distal colon sections from control and HOIP$^{IEC\text{-}\Delta lin}$ mice 24 h post-LPS administration (n=3). Scale bars, 50 μm.

(C) Immunohistochemical staining for CD45 and F4/80 in the distal colon 4 h post-LPS injection (n=3). Data from untreated control (UT) and HOIP$^{IEC\text{-}\Delta lin}$ mice are also shown (n=3). Yellow arrow heads depict cells positive for each marker. Scale bars, 50 μm.

(D) Quantification of immune cells in (C) (n=12 fields per group). Data from untreated control and HOIP$^{IEC\text{-}\Delta lin}$ mice are also shown (n=12 fields per group).

(E) Immunohistochemical staining for cleaved caspase 3 (Cl. Caspase3) in distal colon sections 4 h post-LPS treatment (n=3). Data from untreated control and HOIP$^{IEC\text{-}\Delta lin}$ mice are also shown (n=3). Scale bars, 50 μm.

(F) Immunofluorescence staining for TUNEL (green), E-cadherin (red), and DAPI (blue) in distal colon sections 4 h post-LPS treatment (n=3). Data from untreated control and HOIP$^{IEC\text{-}\Delta lin}$ mice are also shown (n=3). Scale bars, 50 μm.

Statistical significance was determined by two-way ANOVA with Bonferroni's post-hoc test (A, D). $^{*}P < 0.05$, $^{**}P < 0.01$, $^{***}P < 0.005$, $^{****}P < 0.001$.

Figure 2. Intestinal epithelial organoids lacking LUBAC catalytic activity show evidence of apoptosis upon treatment with TNF.

(A) Representative images (top) obtained under a bright field microscope, SYTOX Green staining, and Hoechst 33342 staining of organoids from control and HOIP$^{IEC\text{-}\Delta lin}$ IECs treated

with PBS, LPS (100 ng/ml), or TNF (25 ng/ml) for 24 h. Percentage (bottom) of SYTOX Green-positive organoids among total organoids. Data were obtained from a total of 30–50 organoids per group. Experiments were performed at least three times independently. Scale bars, 100 μm.

(B) ELISA to detect serum TNF levels in control and HOIP$^{IEC\text{-}\Delta lin}$ mice after intraperitoneal injection of LPS (n=3).

(C) qRT-PCR analysis of *Tnf* mRNA levels in colon tissue from control and HOIP$^{IEC\text{-}\Delta lin}$ mice after LPS administration (n=6). Data are normalized to expression of *Gapdh* mRNA.

(D) Organoids derived from control and HOIP$^{IEC\text{-}\Delta lin}$ mice were stimulated with TNF (40 ng/ml), or pre-treated with ZVAD (20μM) for 1 h followed by treatment with TNF (40 ng/ml) for the indicated times. Cell lysates were immunoblotted with the indicated antibodies. Tubulin was used as a loading control.

(E) Organoids from control and HOIP$^{IEC\text{-}\Delta lin}$ mice were stimulated with TNF (40 ng/ml) for the indicated times. Cell lysates were immunoblotted with the indicated antibodies. Tubulin was used as a loading control.

(F) Organoids from control and HOIP$^{IEC\text{-}\Delta lin}$ IECs were stimulated with TNF (25 ng/ml) for the indicated times, followed by qRT-PCR analysis of NF-κB target gene mRNA (n=3). Data are normalized to expression of *Gapdh* mRNA.

A representative image of an immunoblot from at least three independent experiments is shown. Statistical significance was determined by two-way ANOVA with Bonferroni's post-hoc test (A, B, C, F). $^{*}P < 0.05$, $^{***}P < 0.005$, $^{****}P < 0.001$.

Figure 3. TNF plays a role in mucosal inflammation and IEC death in LPS-treated mice lacking linear ubiquitination activity in IECs.

(A) Representative pictures (left) and quantification of colon length (right) in control and HOIP$^{IEC\text{-}\Delta lin}$ mice at the indicated times after intraperitoneal administration of TNF (n=3).

(B) H&E staining of distal colon sections from control and HOIP$^{IEC-\Delta lin}$ mice 24 h after TNF treatment (n=3). Scale bars, 50 μm.

(C) Immunohistochemical staining for CD45 and F4/80 in distal colon sections 4 h after injection of TNF (n=3). Yellow arrow heads indicate cells positive for each marker. Scale bars, 50 μm.

(D) Quantification of immune cells in (C) (n=12 fields per group).

(E) Immunohistochemical staining for cleaved caspase 3 in distal colon from control and HOIP$^{IEC-\Delta lin}$ mice 4 h after TNF treatment (n=3). Scale bars, 50 μm.

(F) HOIP$^{IEC-\Delta lin}$ mice were injected intraperitoneally with isotype control IgG or an anti-TNF antibody 1 h prior to intraperitoneal injection of LPS. Representative pictures (left) and quantification of colon length (right) in isotype control- or anti-TNF-treated HOIP$^{IEC-\Delta lin}$ mice at the indicated times after LPS injection (n=3).

(G) H&E staining of the distal colon sections from isotype control- or anti-TNF-treated HOIP$^{IEC-\Delta lin}$ mice 24 h post-LPS administration (n=3). Scale bars, 50 μm.

(H) Immunohistochemical staining for CD45 and F4/80 in distal colon sections from isotype control- or anti-TNF-treated HOIP$^{IEC-\Delta lin}$ mice 4 h post-LPS (n=3). Yellow arrow heads depict cells positive for each marker. Scale bars, 50 μm.

(I) Quantification of immune cells in (H) (n=12 fields per group).

(J) Immunohistochemical staining for cleaved caspase 3 in distal colon sections from isotype control- or anti-TNF-treated HOIP$^{IEC-\Delta lin}$ mice 4 h after LPS administration (n=3). Scale bars, 50 μm.

Statistical significance was determined by two-way ANOVA with Bonferroni's post-hoc test (A, F), or by a two-tailed unpaired Student's t test (D, I). $^{*}P < 0.05$, $^{**}P < 0.01$, $^{****}P < 0.001$.

Figure 4. Defects in epithelial linear ubiquitination activity do not overtly affect the

severity of DSS-induced colitis.

(A) Control and HOIP$^{IEC\text{-}\Delta lin}$ mice were fed 2.0% DSS for 7 days. They were then fed regular water for 2 days. Body weight changes in control (n=7) and HOIP$^{IEC\text{-}\Delta lin}$ mice (n=7) during DSS treatment. BW, body weight; IBW, initial body weight.

(B) Representative pictures (left) and quantification of colon length (right) in DSS-treated control (n=7) and HOIP$^{IEC\text{-}\Delta lin}$ mice (n=7). Data from untreated control and HOIP$^{IEC\text{-}\Delta lin}$ mice are also shown (n=6).

(C) H&E staining (left) and histological damage scores (right) for distal colon sections from control and HOIP$^{IEC\text{-}\Delta lin}$ mice treated with DSS (n=7). Scale bars, 50 μm.

(D) qRT-PCR analysis of inflammatory cytokine and chemokine expression in colon tissue from control (n=8) and HOIP$^{IEC\text{-}\Delta lin}$ mice (n=6) subjected to DSS-induced colitis. Data from untreated control and HOIP$^{IEC\text{-}\Delta lin}$ mice are also shown (n=3). Data are normalized to expression of *Gapdh* mRNA.

(E) Immunohistochemical staining for cleaved caspase 3 and immunofluorescence staining for TUNEL in distal colon sections from control and HOIP$^{IEC\text{-}\Delta lin}$ mice treated with DSS (n=3). Yellow arrow heads depict cells positive for cleaved caspase 3. Scale bars, 50 μm.

Statistical significance was determined by two-way ANOVA with Bonferroni's post-hoc test (A, B, D), or by a two-tailed unpaired Student's t test (C).

Figure 5. Loss of linear ubiquitination activity in macrophages results in mild colitis after DSS treatment.

(A) Body weight changes in control (n=10) and HOIP$^{MYE\text{-}\Delta lin}$ (n=13) mice during DSS treatment.

(B) Representative pictures (left) and quantification of colon length (right) in DSS-treated control (n=8) and HOIP$^{MYE\text{-}\Delta lin}$ (n=10) mice. Data from untreated control and HOIP$^{MYE\text{-}\Delta lin}$ mice are also shown (n=6).

(C) H&E staining (left) and histological damage scores (right) for distal colon from control and HOIP$^{MYE-\Delta lin}$ mice treated with DSS (n=5). Scale bars, 50 μm.

(D) Immunohistochemical staining for CD45, F4/80, B220, and CD3 in distal colon sections from DSS-treated control and HOIP$^{MYE-\Delta lin}$ mice (n=5). Yellow arrow heads indicate cells positive for each marker. Scale bars, 50 μm.

(E) Quantification of immune cells in (D) (n=10 fields per group). Data from control and HOIP$^{MYE-\Delta lin}$ mice under basal conditions are also shown (n=6 fields per group).

(F) qRT-PCR analysis of inflammatory cytokine and chemokine expression in colon tissue from DSS-treated control (n=5) and HOIP$^{MYE-\Delta lin}$ (n=6) mice. Data from control and HOIP$^{MYE-\Delta lin}$ mice under basal conditions are also shown (n=3). Data are normalized to expression of *Gapdh* mRNA.

Statistical significance was determined by two-way ANOVA with Bonferroni's post-hoc test (A, B, E, F), or by a two-tailed unpaired Student's t test (C). $^{*}P < 0.05$, $^{**}P < 0.01$, $^{****}P < 0.001$.

Figure 6. Deficiency of linear ubiquitination in macrophages impairs NF-κB- and ERK-mediated inflammatory responses upon TLR stimulation.

(A) BMDMs derived from control and HOIP$^{MYE-\Delta lin}$ mice were stimulated with TNF (1 ng/ml) for the indicated times. Cell lysates were immunoblotted with the indicated antibodies. Tubulin was used as a loading control.

(B and C) Control and HOIP$^{MYE-\Delta lin}$ BMDMs were stimulated with LPS (10 ng/ml) for the indicated times. Whole cell lysates were immunoblotted with the indicated antibodies. Tubulin was used as a loading control.

(D) BMDMs from WT mice were pre-treated with DMSO or HOIPin-8 (10 μM) for 30 min, and then stimulated with LPS (10 ng/ml) for the indicated times. Whole cell lysates were immunoblotted with the indicated antibodies. Tubulin was used as a loading control.

(E) ELISA to detect IL-6, TNF, and MCP-1/CCL2 produced by control and HOIP$^{MYE\text{-}\Delta lin}$ BMDMs stimulated with LPS (10 ng/ml) for 24 h (n=3).

(F) BMDMs from WT mice were pre-treated for 30 min with DMSO or HOIPin-8 (10 μM), and then stimulated with LPS (10 ng/ml) for 24 h. Secreted IL-6, TNF, and MCP-1/CCL2 were quantified by ELISA (n=3).

(G) BMDMs from WT mice were pre-treated with DMSO or a MEK inhibitor (0.5 μM) for 10 min, and then stimulated with LPS (10 ng/ml) for 24 h. Secreted IL-6, TNF, and MCP-1/CCL2 were quantified by ELISA (n=3).

(H) Control and HOIP$^{MYE\text{-}\Delta lin}$ BMDMs were stimulated for 24 h with the indicated TLR ligands. Secreted IL-6 was measured by ELISA (n=3). The concentrations of the TLR ligands were as follows: Poly(I:C) (2 μg/ml), CpG-B (5 μM), and Pam3CSK4 (1 μg/ml).

A representative image of an immunoblot from at least three independent experiments is shown.

Statistical significance was determined by a two-tailed unpaired Student's t test (E, F, G, H). $^{*}P < 0.05$, $^{**}P < 0.01$, $^{***}P < 0.005$, $^{****}P < 0.001$.

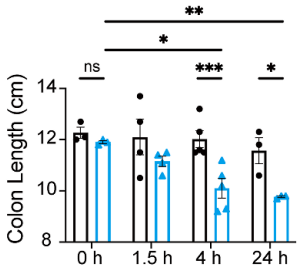

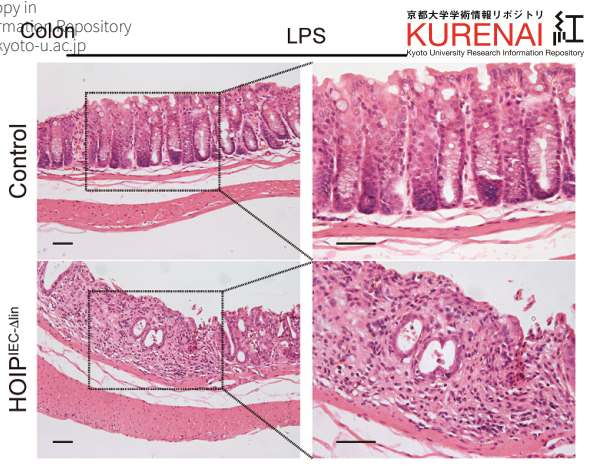

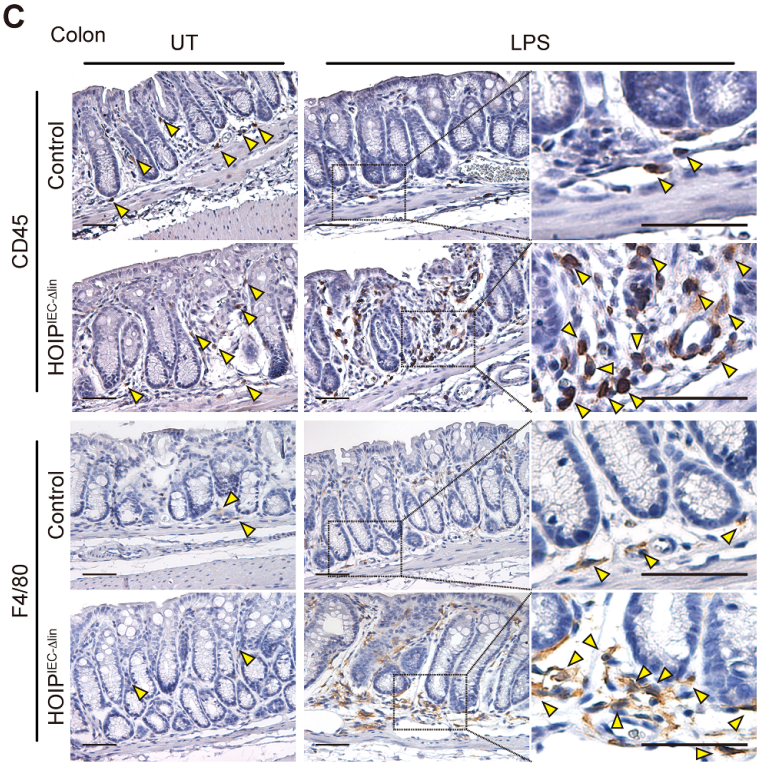

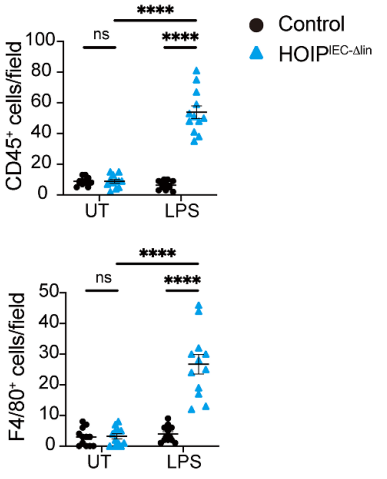

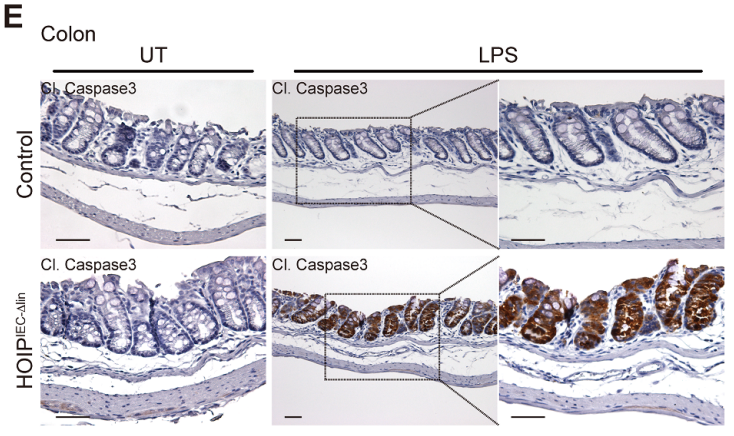

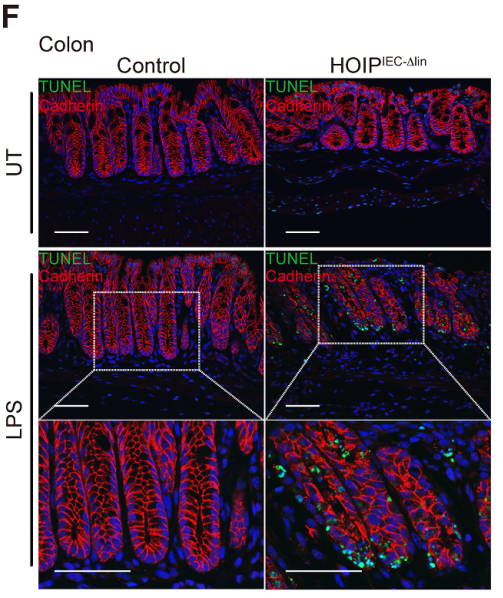

Figure 1

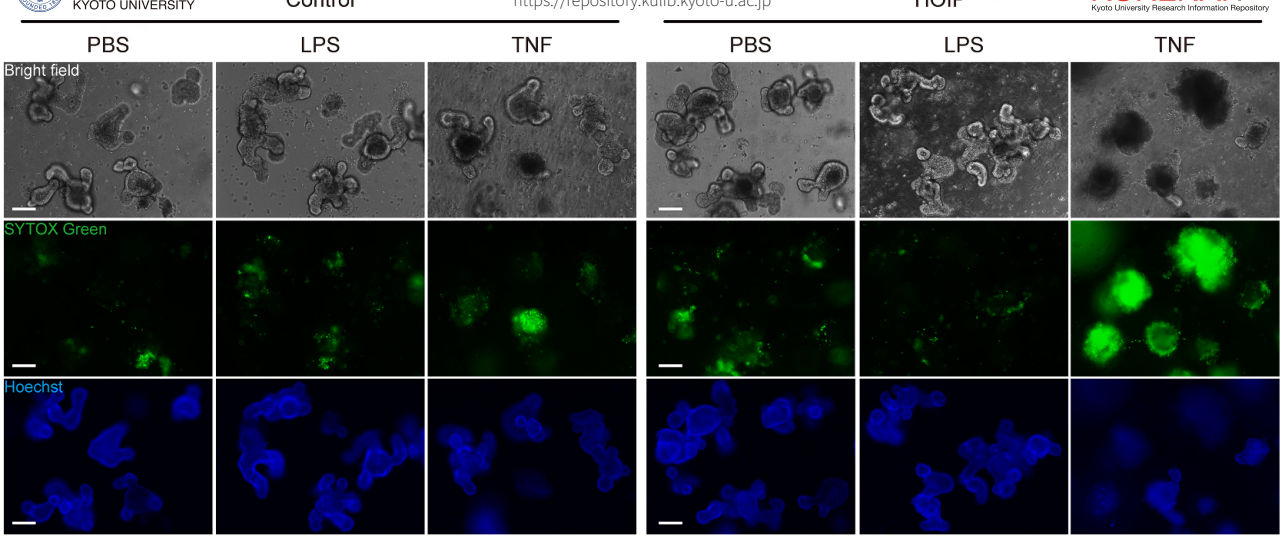

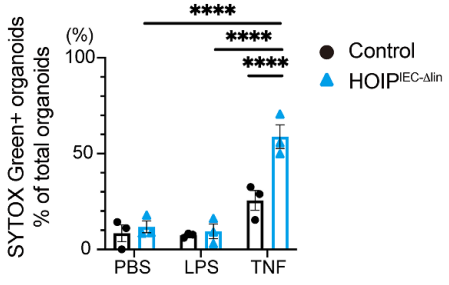

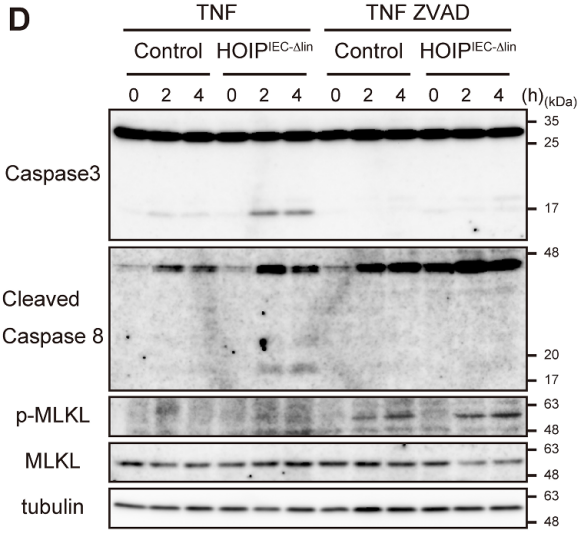

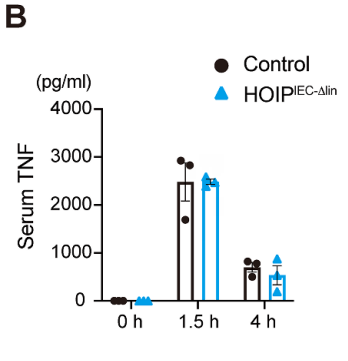

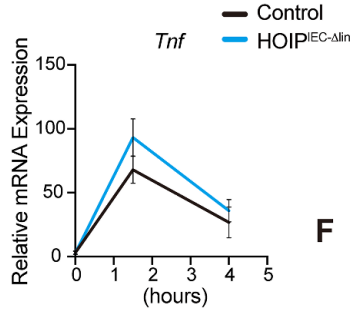

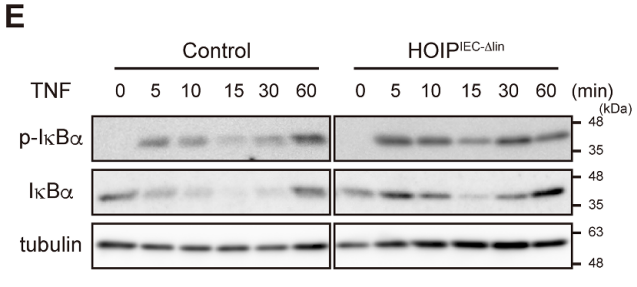

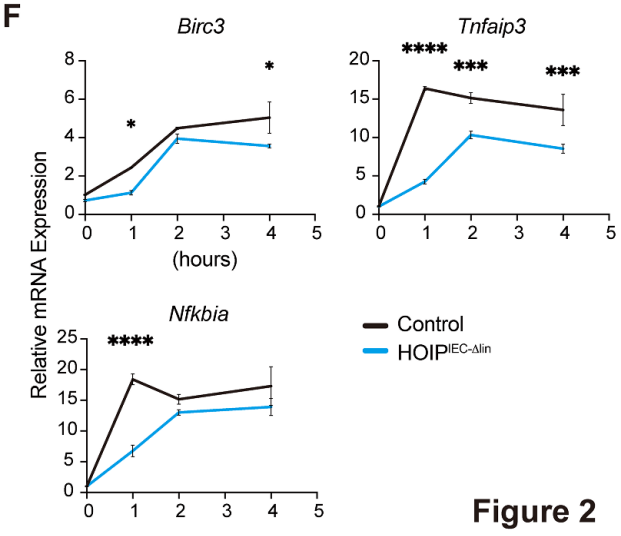

Figure 2

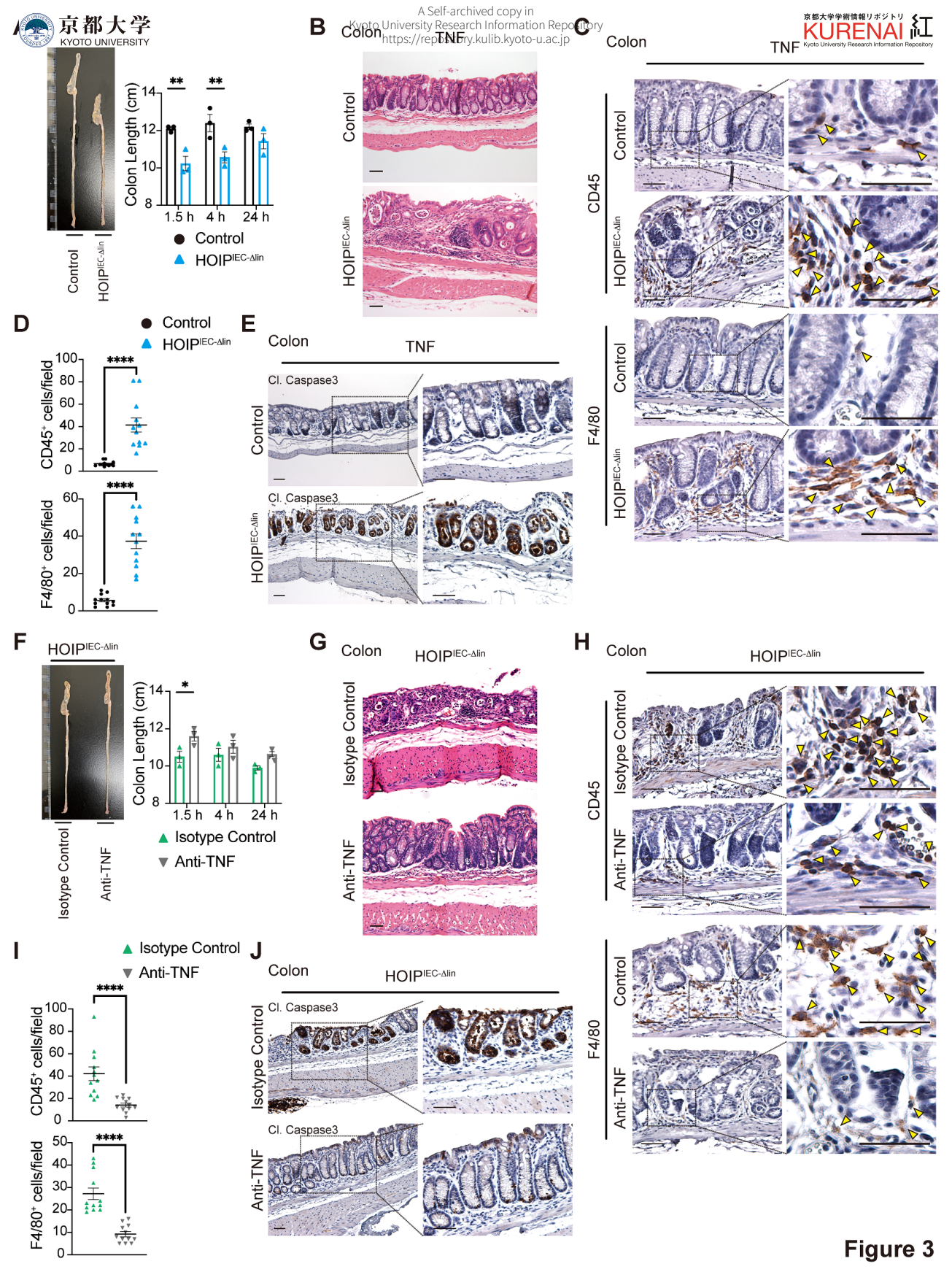

Figure 3

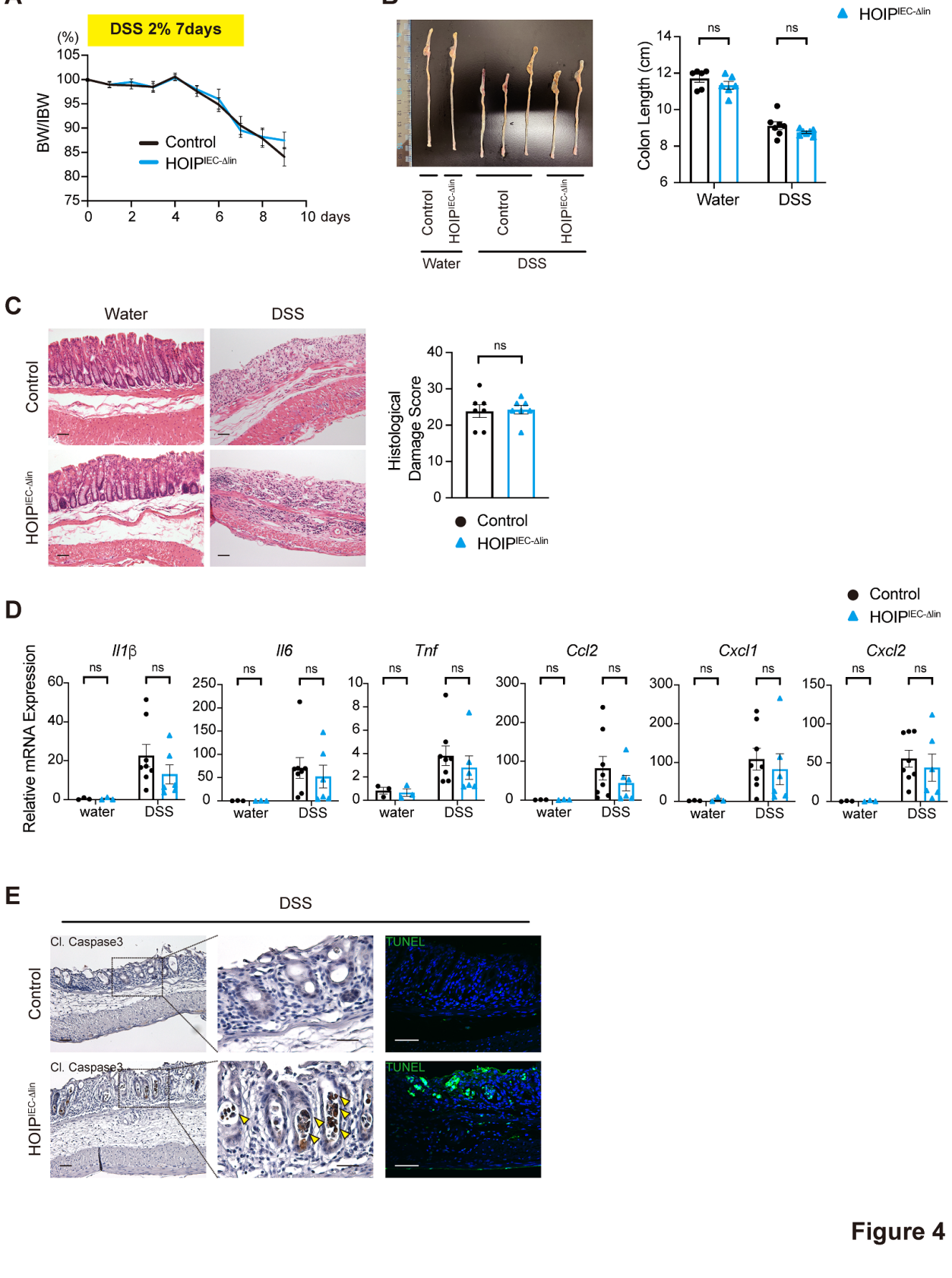

Figure 4

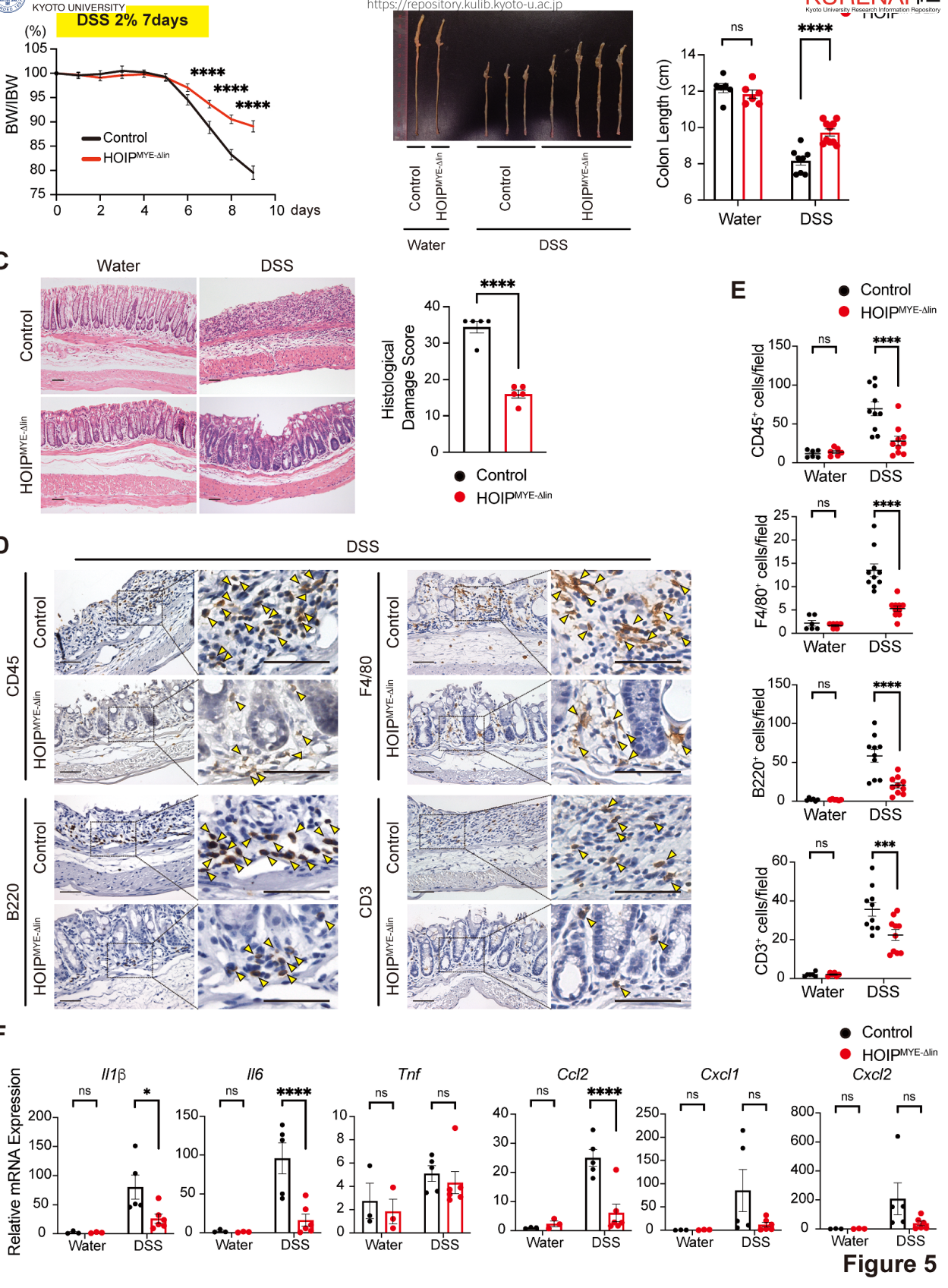

Figure 5

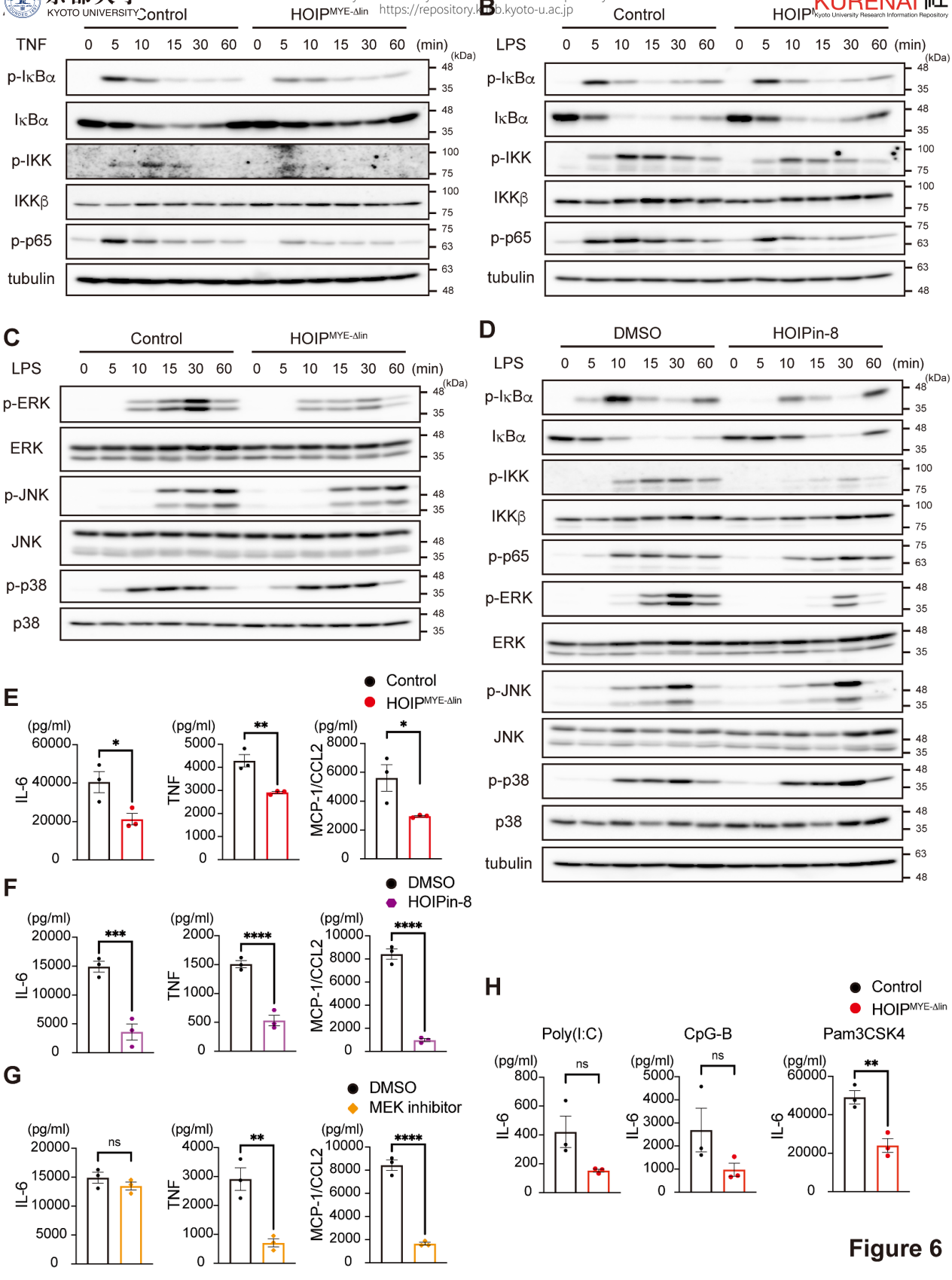

Figure 6

Supporting Information

Supplementary materials and methods

Antibodies

The following antibodies were used for immunohistochemistry: anti-CD45 (clone 30F-11, cat. no. 550539, 1:100 dilution; BD Biosciences, Franklin Lakes, NJ, USA), anti-F4/80 (clone CI:A3-1, cat. no. MCA497GA, 1:100 dilution; Bio-Rad, Hercules, CA, USA), anti-cleaved caspase-3 (cat. no. 9661, 1:100 dilution; Cell Signaling Technology, Danvers, MA, USA), anti-CD45R/B220 (clone RA3-6B2, cat. no. 103202, 1:200 dilution; BioLegend, San Diego, CA, USA), and anti-CD3ε (clone M-20, cat. no. SC-1127, 1:400 dilution; Santa Cruz Biotechnology, Dallas, TX, USA). The following antibodies were used for immunofluorescence staining: anti-F4/80 (cat. no. 70076, 1:100 dilution; Cell Signaling Technology), anti-E-Cadherin (cat. no. GTX100443, 1:50 dilution; Gene Tex, Irvine, CA, USA), anti-CD3ε (clone M-20, cat. no. SC-1127, 1:400 dilution; Santa Cruz Biotechnology); anti-rabbit IgG AlexaFlour 488 (cat. no. A-11034), anti-rabbit IgG-AlexaFluor 546 (cat. no. A-11035), and anti-goat IgG AlexaFlour 488 (cat. no. A-11055) (all from Invitrogen, Waltham, MA, USA; 1:200 dilution). The following antibodies were used for immunoblotting: anti-IκBα (cat. no. 4812), anti-p-IκBα (cat. no. 9246), anti-IKKβ (cat. no. 8943), anti-p-IKK (cat. no. 2697), anti-p-p65 (cat. no. 3033), anti-ERK (cat. no. 9102), anti-p-ERK (cat. no. 9101), anti-JNK (cat. no. 9258), anti-p-JNK (cat. no. 4668), anti-p38 (cat. no. 9212), anti-p-p38 (cat. no. 9211), anti-caspase-3 (cat. no. 9662), anti-cleaved caspase-8 (cat. no. 8592) (all from Cell Signaling Technology; 1:2000 dilution); anti-MLKL (phosphor S345) (cat. no. ab196436, 1:2000 dilution; abcam, Waltham, MA, USA), anti-MLKL (cat. no. SAB1302339, 1:250 dilution; Sigma-Aldrich, St. Louis, MO, USA); anti-mouse HOIP (clone N1), anti-HOIL-1L (clone 2E2), anti-SHARPIN (clone lot1) (all produced in-house; 1:2000 dilution); β-actin (clone AC-74, cat. no. A5316, 1:5000 dilution; Sigma-Aldrich), α-tubulin

(clone DM1A, cat. no. CLT9002, 1:5000 dilution; CEDARLANE, Ontario, Canada), HRP-linked anti-rabbit IgG (cat. no. NA934V, 1:5000 dilution; Cytiva, Marlborough, MA, USA), and HRP-linked anti-mouse IgG (cat. no. 7076, Cell Signaling Technology; 1:5000 dilution). The following antibodies were used for flow cytometry analysis: APC-Cy7-anti-CD45 (clone 30F-11, cat. no. 103116, 1:100 dilution), APC-anti-F4/80 (clone BM8, cat. no. 123115, 1:200 dilution), PE-Cy7-anti-CD11b (clone M1/70, cat. no. 101215, 1:200 dilution), PE-Cy7-anti-CD19 (clone 6D5, cat. no. 115520, 1:200 dilution), PerCP-Cy5-5-anti-CD4 (clone GK1.5, cat. no. 100434, 1:200 dilution), PE-Cy7-anti-CD8a (clone 53-6.7, cat. no. 100722, 1:200 dilution), APC-anti-CD69 (clone H1.2F3, cat. no. 104513, 1:200 dilution), APC-anti-CD62L (clone MEL-14, cat. no. 104412, 1:200 dilution), PE-anti-CD44 (clone IM7, cat. no. 103008, 1:200 dilution), streptavidin-PerCP-Cy5-5 (cat. no. 405213, 1:400 dilution) (all from BioLegend); PE-anti-FAS (clone Jo2, cat. no. 554258, 1:200 dilution; BD Biosciences), FITC-anti-TCRb (clone H57-597, cat. no. 11-5961-82, 1:200 dilution; eBioscience, San Diego, CA, USA), PE-anti-CD25 (clone PC61.5, cat. no. 12-0251-81, 1:200 dilution, eBioscience), and Biotin-anti-PNA (cat. no. B-1075, 1:400 dilution, Vector Laboratories, Newark, CA, USA).

Histological assessment of DSS-induced colitis

The histological damage score was determined based on three parameters. Inflammation severity was scored as 0–3, extent of inflammation was scored as 0–3, and crypt damage was scored as 0–4. The sum of each parameter was multiplied by percentage involvement (0% = 0; ≦25% = 1; ≦50% = 2; ≦75% = 3; and ≦100% = 4) to yield the histological damage score.

Immunostaining

Immunohistochemical staining was performed using an ImmPRESS Polymer Detection Kit

(Vector Laboratories). Paraffin-embedded sections were deparaffinized, rehydrated, and then immersed in citrate buffer (pH 6.0) for 15 min in a microwave processor (MI-77; Azumayaika, Tokyo, Japan) for antigen retrieval. After blocking with normal goat or horse serum blocking solution (Vector Laboratories), sections were incubated with primary antibody overnight at 4℃. The stained sections were incubated for 30 min at room temperature with ImmPRESS Polymer Reagent (Vector Laboratories), then colored with diaminobenzidine substrate (DAKO, Carpinteria, CA, USA) and counterstained with hematoxylin. Endogenous peroxidase was quenched for 10 min at room temperature in 0.45% H_2O_2 in methanol or 3% H_2O_2 in water. Prior to immunofluorescence staining, antigen retrieval was performed as described above. After sections were blocked for 1 h with blocking buffer (2% BSA and 0.1% Triton X-100 in PBS) containing 5% goat serum, sections were incubated overnight at 4°C with primary antibodies diluted in blocking buffer. The stained sections were incubated for 1 h at room temperature with fluorescent dye-conjugated anti-rabbit IgG-AlexaFluor 488 or anti-goat IgG-AlexaFluor 488 in blocking buffer. For preservation, labeled sections were mounted in ProLong Glass Antifade Mountant (Invitrogen). TUNEL staining was performed using an In Situ Cell Death Detection Kit, Fluorescein (Sigma-Aldrich). Prior to co-staining for TUNEL and for E-Cadherin, antigen retrieval was performed as described above. Then, sections were incubated for 1 h at 37°C with TUNEL reaction mixture. After blocking as described above, sections were incubated overnight at 4°C with an anti-E-Cadherin antibody in blocking buffer. The stained sections were then incubated for 1 h at room temperature with fluorescent dye-conjugated anti-rabbit IgG-AlexaFluor 546 in blocking buffer. For preservation, labeled sections were mounted in ProLong Glass Antifade Mountant (Invitrogen). DAPI was used to stain nuclei.

IEC isolation and organoid culture

The distal 10 cm segment of the small intestine or the whole colon was opened longitudinally and minced. The intestinal segments were washed with cold PBS and incubated at 4℃ for 40 min with PBS containing 5 mM EDTA and 10% FBS (whole colon was incubated for 60 min) with rocking. After removal of the EDTA medium, the tissue fragments were shaken vigorously in cold PBS to detach the villous and crypt fractions, and then passed through a 100 μm cell strainer (Corning, Glendale, AZ, USA). For IEC isolation, the flow-through were pelleted and lysed for RNA extraction or immunoblotting. For organoid culture, the flow-through from the small intestine was filtered through a 70 μm cell strainer (Corning) to remove villous material. Isolated crypts were mixed with 50 μl of Matrigel (Corning) and plated in 24-well plates. After the Matrigel polymerized, 500 μl of IntestiCult Organoid Growth Medium (STEMCELL Technologies, Vancouver, Canada) was added to each well, followed by cultivation at 37℃/5% CO_2.

Enrichment of peritoneal macrophages

Peritoneal macrophages were obtained by flushing out the peritoneal cavity with 10 ml of cold PBS. The collected medium was plated into 6 or 12 well plates for 2 h. Non-adherent cells were washed away with PBS and the attached cells were used as peritoneal macrophages. Primary cells from each organ were washed with Gey's Buffer to deplete red blood cells.

Immunoblotting

Cells were lysed with lysis buffer containing 50 mM Tris-HCl (pH 7.5), 150 mM NaCl, 1% Triton X-100, 2 mM PMSF, and protease inhibitor cocktail (Sigma-Aldrich). Organoids were lysed in RIPA buffer (50 mM Tris-HCl (pH 8.0), 150 mM NaCl, 1% Triton X-100, 0.1% SDS, 0.1% sodium deoxycholate, 2 mM PMSF, and protease inhibitor cocktail; (Sigma-Aldrich)). Lysates were centrifuged at 15,000 rpm for 10 min at 4℃, and the supernatant was used in

subsequent steps. To examine phosphorylation, a phosphatase inhibitor cocktail (Nacalai Tesque, Kyoto, Japan) was added. To assess the protein translocating to the nucleus, total cell lysates were obtained by incubation in SDS sample buffer. The cell lysates were then separated by SDS-PAGE and transferred onto PVDF membranes (Merck Millipore, Burlington, MA, USA). After blocking in Tris-buffered saline containing 0.1% Tween 20 and 5% nonfat dry milk, the membrane was immunoblotted with the indicated primary antibodies, followed by the corresponding secondary antibodies. The membranes were visualized by enhanced chemiluminescence and analyzed by an LAS3000 or LAS4000mini instrument (GE Healthcare, Chicago, IL, USA).

Quantitative RT-PCR analysis

Total RNA from IECs or organoids was extracted using an RNeasy Mini Kit (Qiagen, Venlo, Netherlands). To extract RNA from colon tissue, 5 mm segments taken from between the middle and distal third of the colon were used. Pre-purified RNAs were extracted using ISOGEN (NIPPON GENE, Tokyo, Japan), and then subjected to column-based purification using an RNeasy Mini Kit (Qiagen). Total RNA was reverse transcribed into cDNA using a High Capacity RNA-to-cDNA Kit (Thermo Fisher Scientific). Real-time PCR was performed with Power SYBR Green PCR Master Mix (Thermo Fisher Scientific) and a ViiA7 Real-Time PCR system (Applied Biosystems, Waltham, MA, USA). The results were analyzed by the ΔΔCT method. The sequences of the primers used for qPCR are listed in Table S1.

ELISA

Cell culture supernatants and serum were collected and stored at -80°C until use. The concentrations of TNF, IL-6, and MCP-1/CCL2 in culture supernatants and serum were measured using an ELISA MAX Standard Set (BioLegend). BD OPtEIA (BD Biosciences)

was used as the substrate. Absorbance at 450 nm, with a correction wave length of 570 nm, was detected by a microplate reader (Molecular Devices, San Jose, CA, USA).

Flow cytometry

Primary cells isolated from the spleen or peripheral lymph nodes, or BMDMs, were incubated with a mixture of the fluorochrome-conjugated antibodies. Samples were run on FACSCanto Ⅱ (BD Biosciences) using FACS Diva software v.6.1.2 (BD Biosciences). The results were analyzed using FlowJo software v.9.9.6 (Tomy Digital Biology, Tokyo, Japan).

135 **Supplementary figures S1–S11**

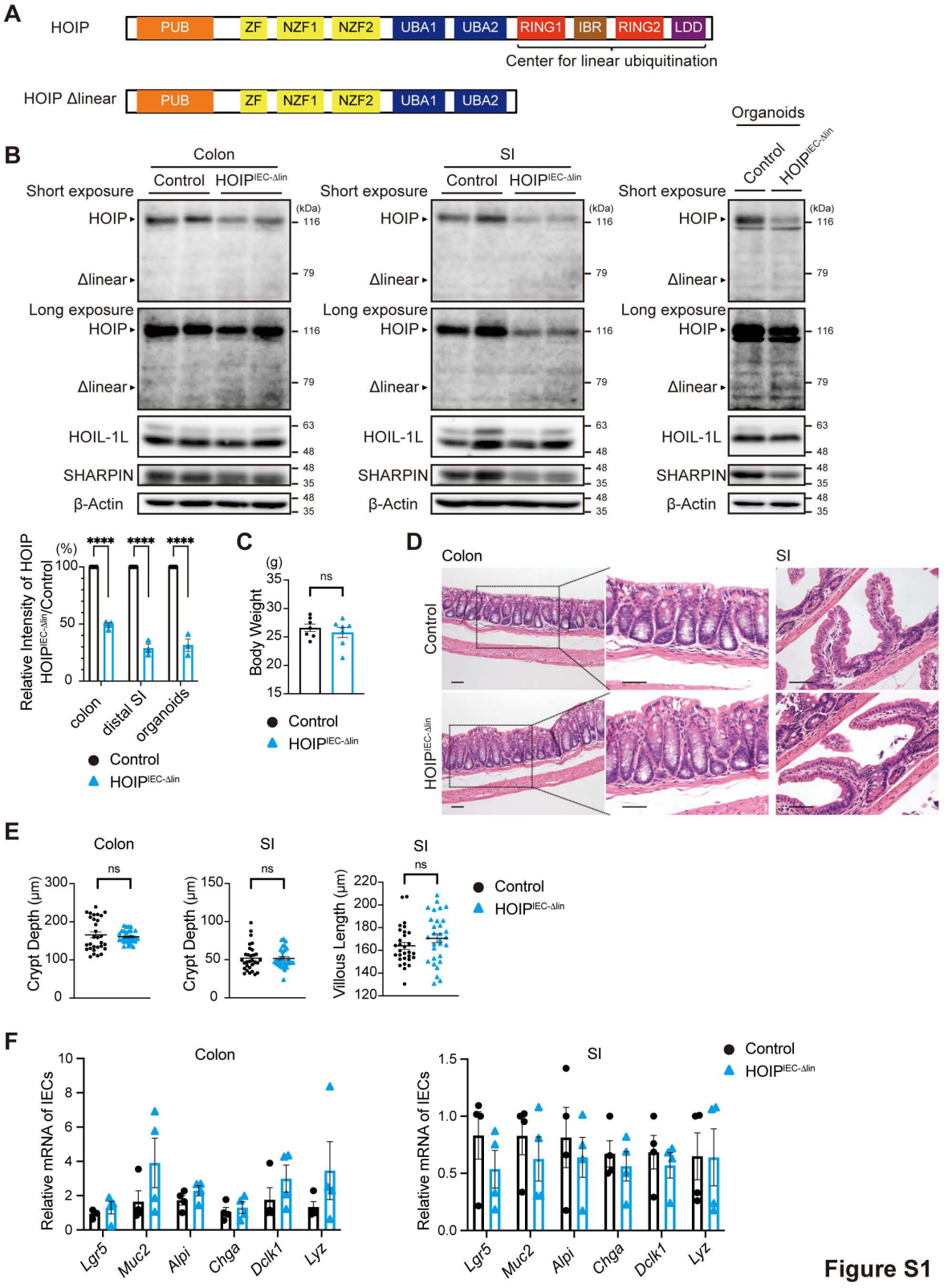

Figure S1

136

137 **Figure S1. No morphological or developmental changes in the intestine of HOIP$^{IEC-\Delta lin}$**

138 **mice under basal conditions.**

(A) Schematic illustration of the target region within the HOIP gene.

(B) Immunoblot analysis (top) of LUBAC subunits in lysates of IECs from the colon and the small intestine (SI) and organoids of control and HOIP$^{IEC-\Delta lin}$ mice. β-actin was used as a loading control. Relative band intensity (bottom) of HOIP in HOIP$^{IEC-\Delta lin}$ mice, normalized to the intensity in littermate controls (n=3).

(C) Body weight of control and HOIP$^{IEC-\Delta lin}$ mice under basal conditions (n=7). ns, not significant.

(D) H&E staining of the colon and the small intestine from control and HOIP$^{IEC-\Delta lin}$ mice (n=3). Scale bars, 50 μm.

(E) Crypt length in the colon and small intestine, and villous length in the small intestine, of control and HOIP$^{IEC-\Delta lin}$ mice (n=30 fields per group).

(F) qRT-PCR analysis of expression of mRNA encoding epithelial markers by IECs from the colon and small intestine of control and HOIP$^{IEC-\Delta lin}$ mice (n=4). Data are normalized to expression of *Gapdh* mRNA.

Statistical significance was determined by two-way ANOVA with Bonferroni's post-hoc test (B, F) or a two-tailed unpaired Student's t test (C, E). $^{****}P < 0.001$.

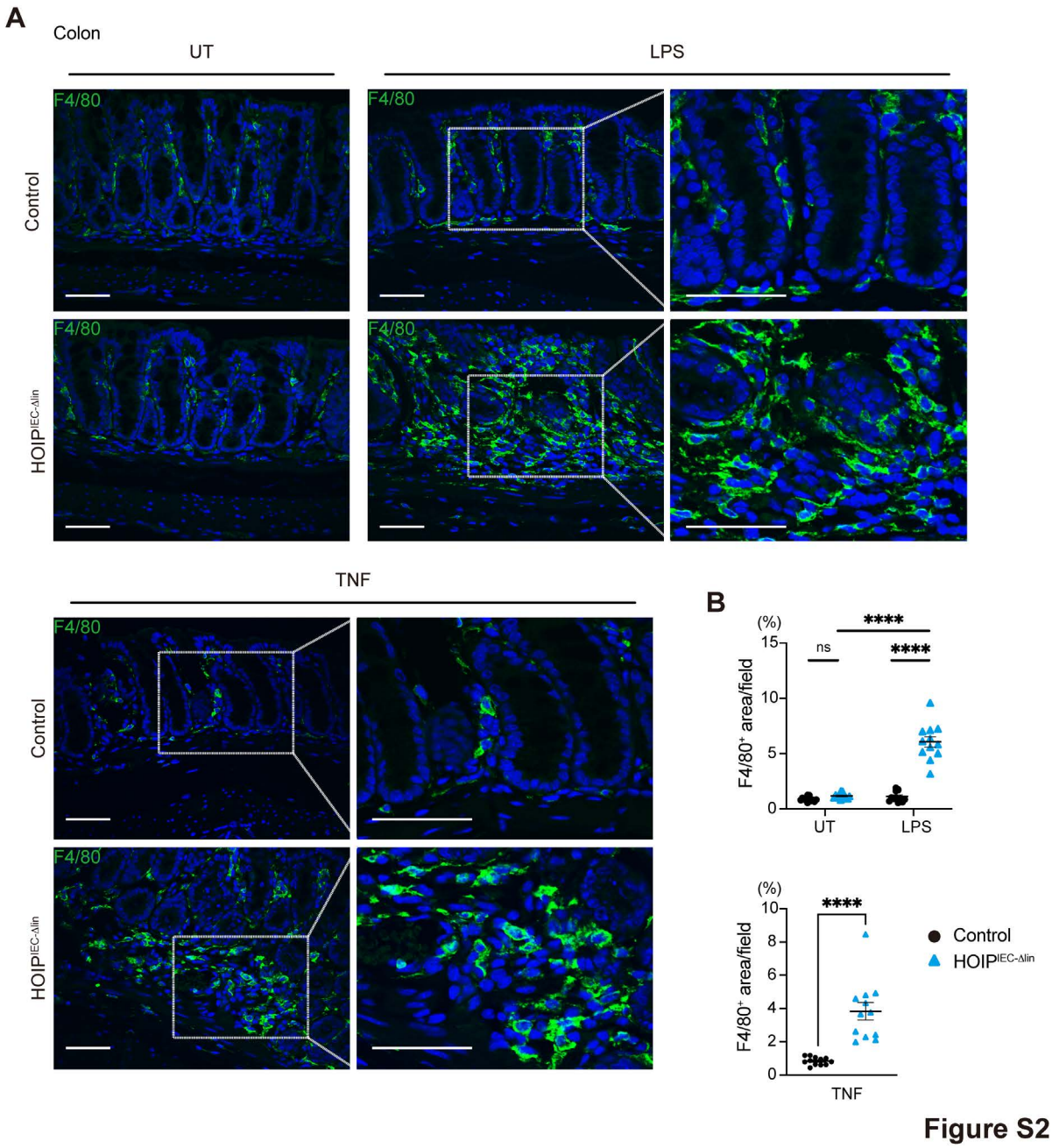

Figure S2

156

157 **Figure S2. Immunofluorescence staining for F4/80 in distal colon sections from control**

158 **and HOIP$^{IEC-\Delta lin}$ mice after injection of LPS or TNF.**

159 (A) Immunofluorescence staining for F4/80 in the distal colon 4 h post-injection of LPS or

160 TNF (n=3). Data from untreated control (UT) and HOIP$^{IEC-\Delta lin}$ mice are also shown (n=3).

161 Scale bars, 50 μm.

162 (B) Quantification of the F4/80^{+} cells in (A) (n=12 fields per group).

163 Statistical significance was determined by two-way ANOVA with Bonferroni's post-hoc

test (B, top), or a two-tailed unpaired Student's t test (B, bottom). ****P < 0.001.

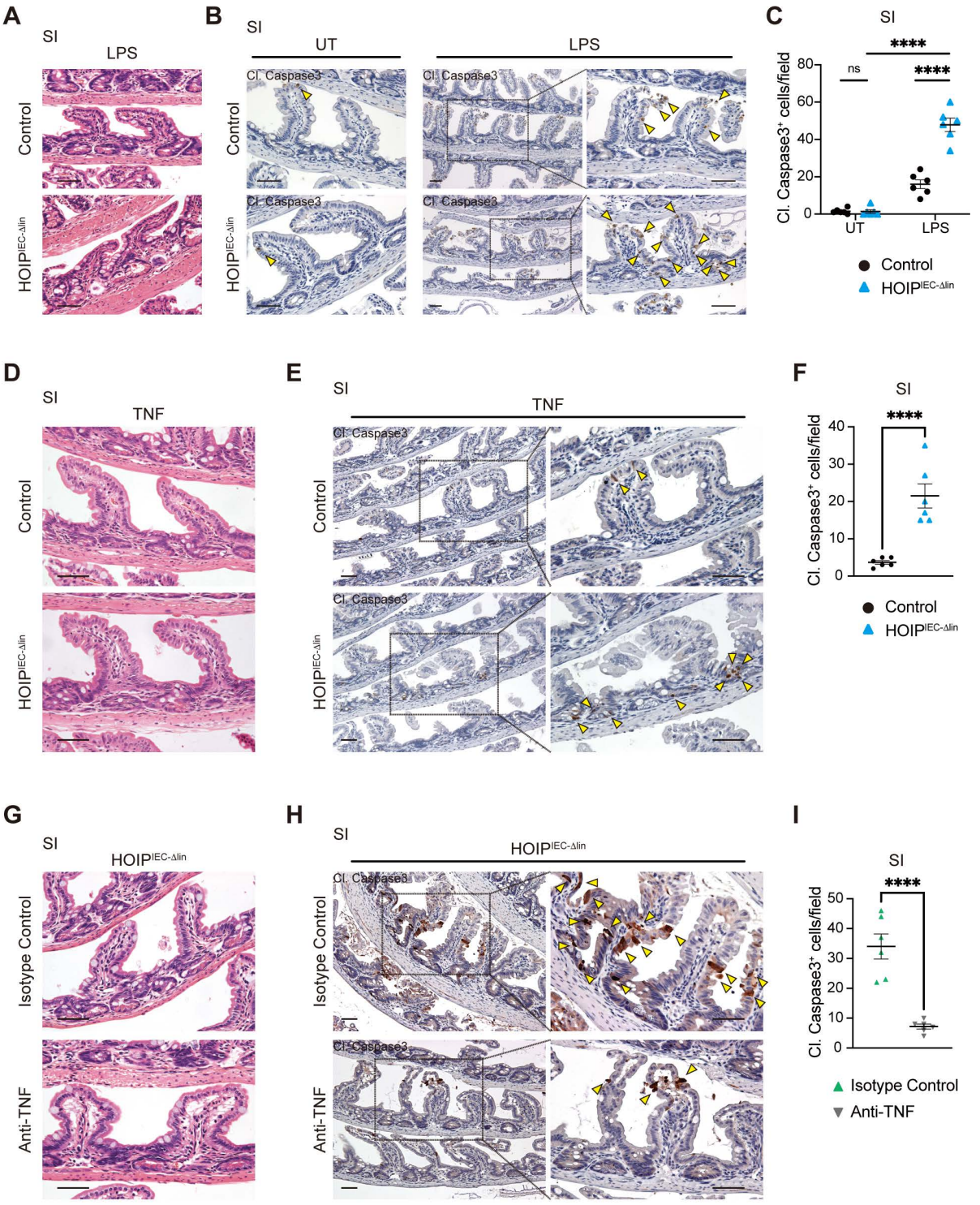

Figure S3

Figure S3. TNF mediates IEC death in the small intestine of HOIP$^{IEC-\Delta lin}$ mice upon LPS administration.

(A) H&E staining of small intestine sections from control and HOIP$^{IEC-\Delta lin}$ mice 24 h after LPS administration (n=3). Scale bars, 50 μm.

(B) Immunohistochemical staining of cleaved caspase 3 (Cl. Caspase3) in sections of small intestine at 1.5 h post-LPS treatment (n=3). Data of untreated control and HOIP$^{IEC-\Delta lin}$ mice are also shown (n=3). Yellow arrow heads show cells positive for cleaved caspase 3 in the small intestine. Scale bars, 50 μm.

(C) Number of cleaved caspase 3-positive cells in the small intestine (n=6 fields per group).

(D) H&E staining of small intestine sections from control and HOIP$^{IEC-\Delta lin}$ mice 24 h after TNF treatment (n=3). Scale bars, 50 μm.

(E) Immunohistochemical staining of cleaved caspase 3 in the small intestine of control and HOIP$^{IEC-Dlin}$ mice 1.5 h post-TNF treatment (n=3). Yellow arrow heads show cells positive for cleaved caspase 3. Scale bars, 50 μm.

(F) Number of cleaved caspase 3-positive cells in the small intestine (n=6 fields per group).

(G) H&E staining of the small intestine sections from isotype control- or anti-TNF-treated HOIP$^{IEC-\Delta lin}$ mice 24 h post-LPS administration (n=3). Scale bars, 50 μm.

(H) Immunohistochemical staining for cleaved caspase 3 in the small intestine of isotype control- or anti-TNF-treated HOIP$^{IEC-\Delta lin}$ mice 1.5 h post-LPS administration (n=3). Yellow arrow heads show cells positive for cleaved caspase 3. Scale bars, 50 μm.

(I) Number of cleaved caspase 3-positive cells in the small intestine (n=6 fields per group).

Statistical significance was determined by two-way ANOVA with Bonferroni's post-hoc test (C), or a two-tailed unpaired Student's t test (F, I). $^{****}P < 0.001$.

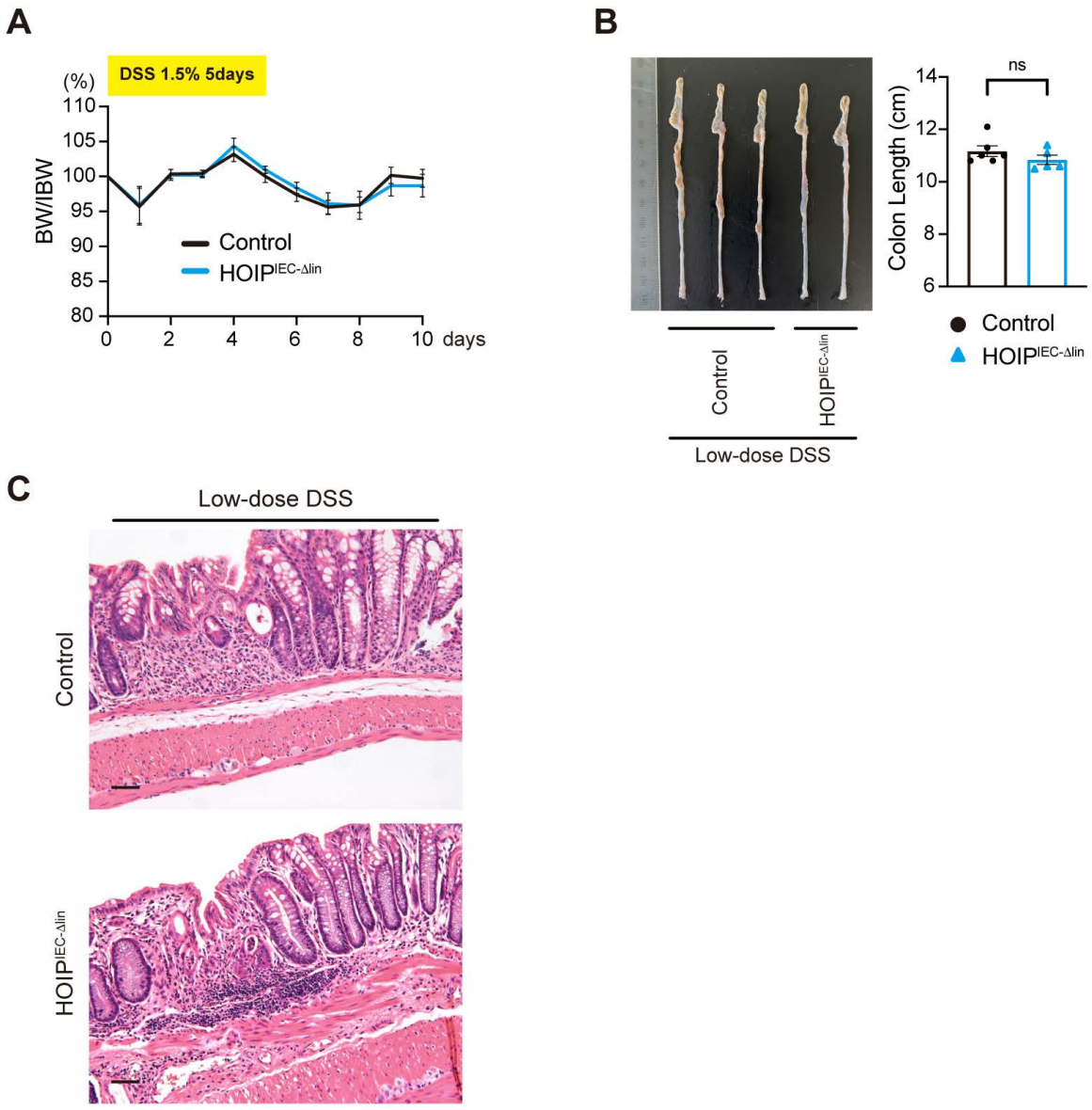

Figure S4

Figure S4. Loss of linear ubiquitination activity in IECs does not overtly affect the severity of low-dose DSS-indued colitis.

(A) Control and HOIP$^{IEC\text{-}\Delta lin}$ mice were fed 1.5% DSS for 5 days. They were then fed regular water for 5 days. Body weight changes in control (n=6) and HOIP$^{IEC\text{-}\Delta lin}$ mice (n=5) were measured during DSS treatment. BW, body weight; IBW, initial body weight.

(B) Representative pictures (left) and quantification of colon length (right) in DSS-treated control (n=6) and HOIP$^{IEC\text{-}\Delta lin}$ mice (n=5).

(C) H&E staining of distal colon sections from control and HOIP$^{IEC\text{-}\Delta lin}$ mice treated with

DSS (n=5). Scale bars, 50 μm.

Statistical significance was determined by two-way ANOVA with Bonferroni's post-hoc test (A), or by a two-tailed unpaired Student's t test (B).

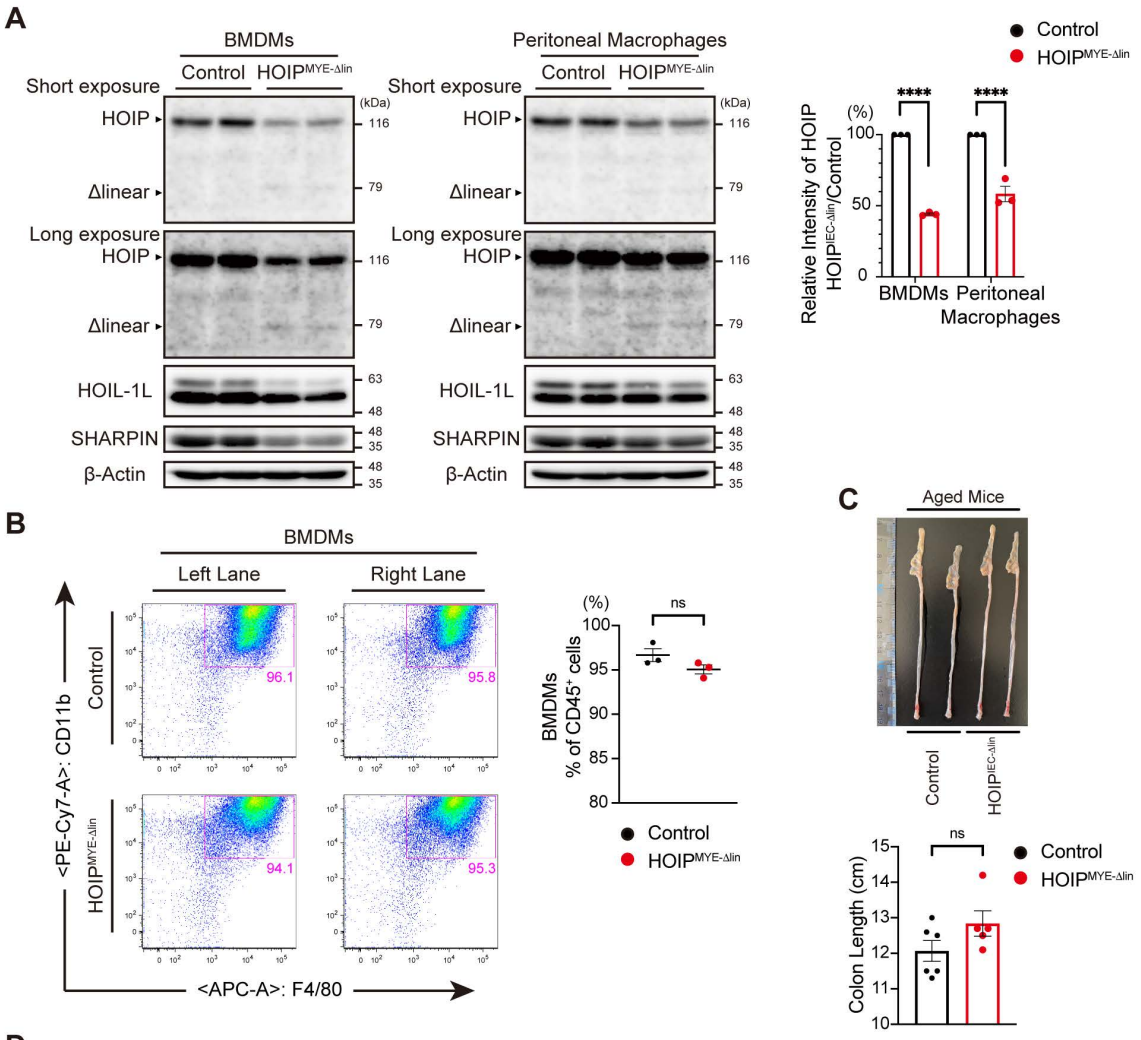

Figure S5

Figure S5. Aged HOIP$^{MYE-\Delta lin}$ mice do not show inflammatory or autoimmune phenotypes under basal conditions.

(A) Immunoblot analysis (left) of LUBAC subunits in lysates of BMDMs and peritoneal

208 macrophages from control and HOIP$^{MYE-\Delta lin}$ mice. β-actin was used as a loading control.
209 Relative band intensity (right) of HOIP in HOIP$^{IEC-\Delta lin}$ mice, normalized to the intensity in
210 littermate controls (n=3).
211 (B) Flow cytometry analysis of BMDM differentiation in (A) (left), and the proportion of
212 differentiated BMDMs (F4/80^{+}CD11b^{+}) among CD45^{+} cells (n=3) (right).
213 (C) Representative pictures (top), and quantification of colon length (bottom), from aged
214 control (n=6) and HOIP$^{MYE-\Delta lin}$ mice (n=5). Aged mice were 24–32 weeks old.
215 (D) H&E staining of the colon, small intestine, and skin from aged control and HOIP$^{MYE-\Delta lin}$
216 mice (n=3). Scale bars, 50 μm.
217 Statistical significance was determined by two-way ANOVA with Bonferroni's post hoc-test
218 (A) or a two-tailed unpaired Student's t test (B, C). $^{****}P < 0.001$.
219

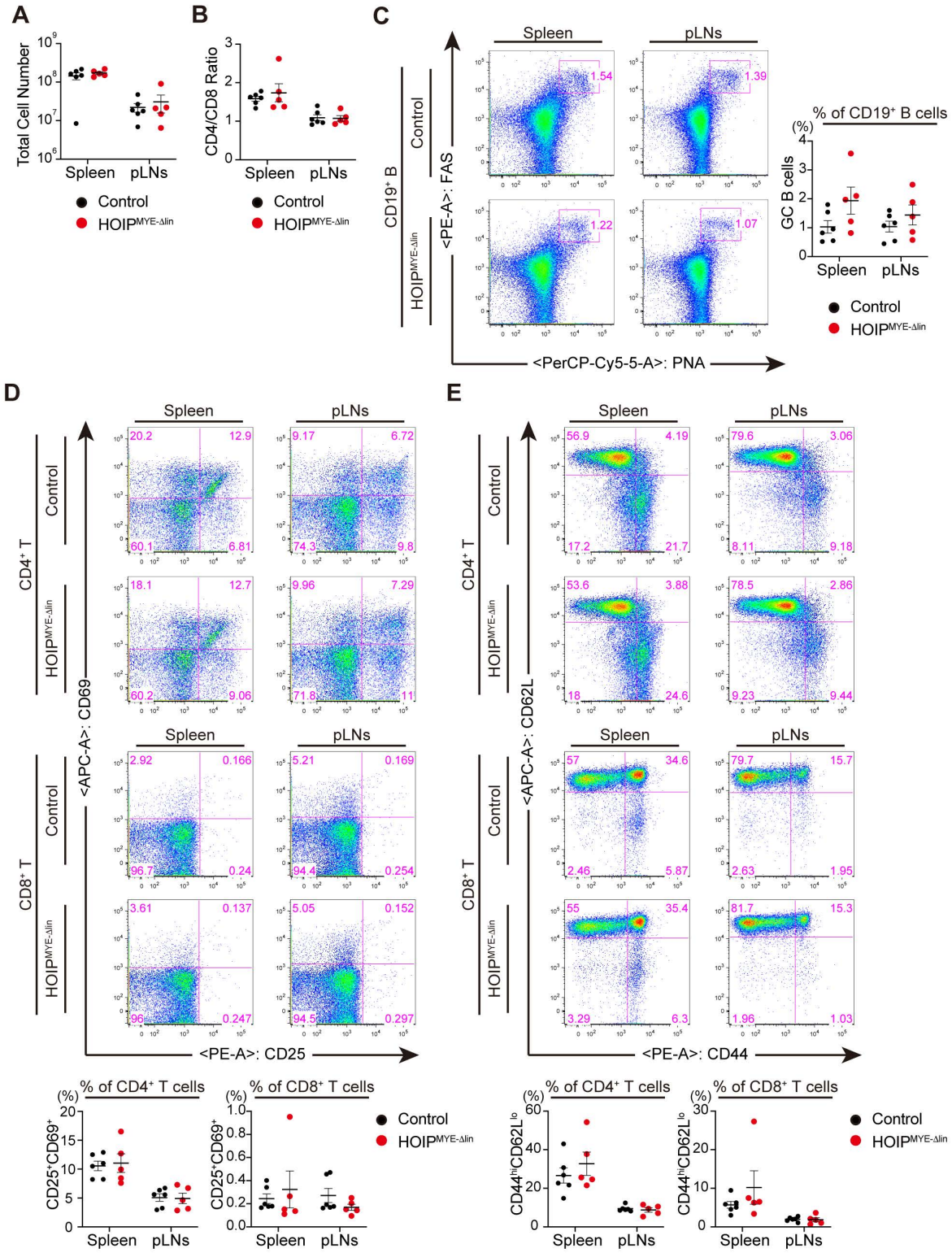

Figure S6

Figure S6. No overt changes in the proportion of activated lymphocytes in aged HOIP$^{MYE-\Delta lin}$ mice under basal conditions.

(A) Total number of immune cells in the spleen and peripheral lymph nodes (pLNs) from

aged control (n=6) and HOIP$^{MYE-\Delta lin}$ mice (n=5).

(B) Flow cytometry analysis of the CD4/CD8 T cell ratio in aged control (n=6) and HOIP$^{MYE-\Delta lin}$ mice (n=5).

(C) Representative flow cytometry plots (left) and percentages (right) of germinal center (GC) B cells (PNA^{+}FAS^{+}) within the CD19^{+} B cell population in the spleen and pLNs of aged control (n=6) and HOIP$^{MYE-\Delta lin}$ mice (n=5).

(D) Representative flow cytometry plots (top) and percentages (bottom) of activated T cells (CD25^{+}CD69^{+}) in the CD4^{+} and CD8^{+} T cell populations in the spleen and pLNs of aged control (n=6) and HOIP$^{MYE-\Delta lin}$ mice (n=5).

(E) Representative flow cytometry data (top) and percentages (bottom) of effector T cells (CD44^{hi}CD62L^{lo}) in the CD4^{+} and CD8^{+} T cell populations in the spleen and pLNs of aged control (n=6) and HOIP$^{MYE-\Delta lin}$ mice (n=5).

Statistical significance was determined by two-way ANOVA with Bonferroni's post hoc-test (A–E).

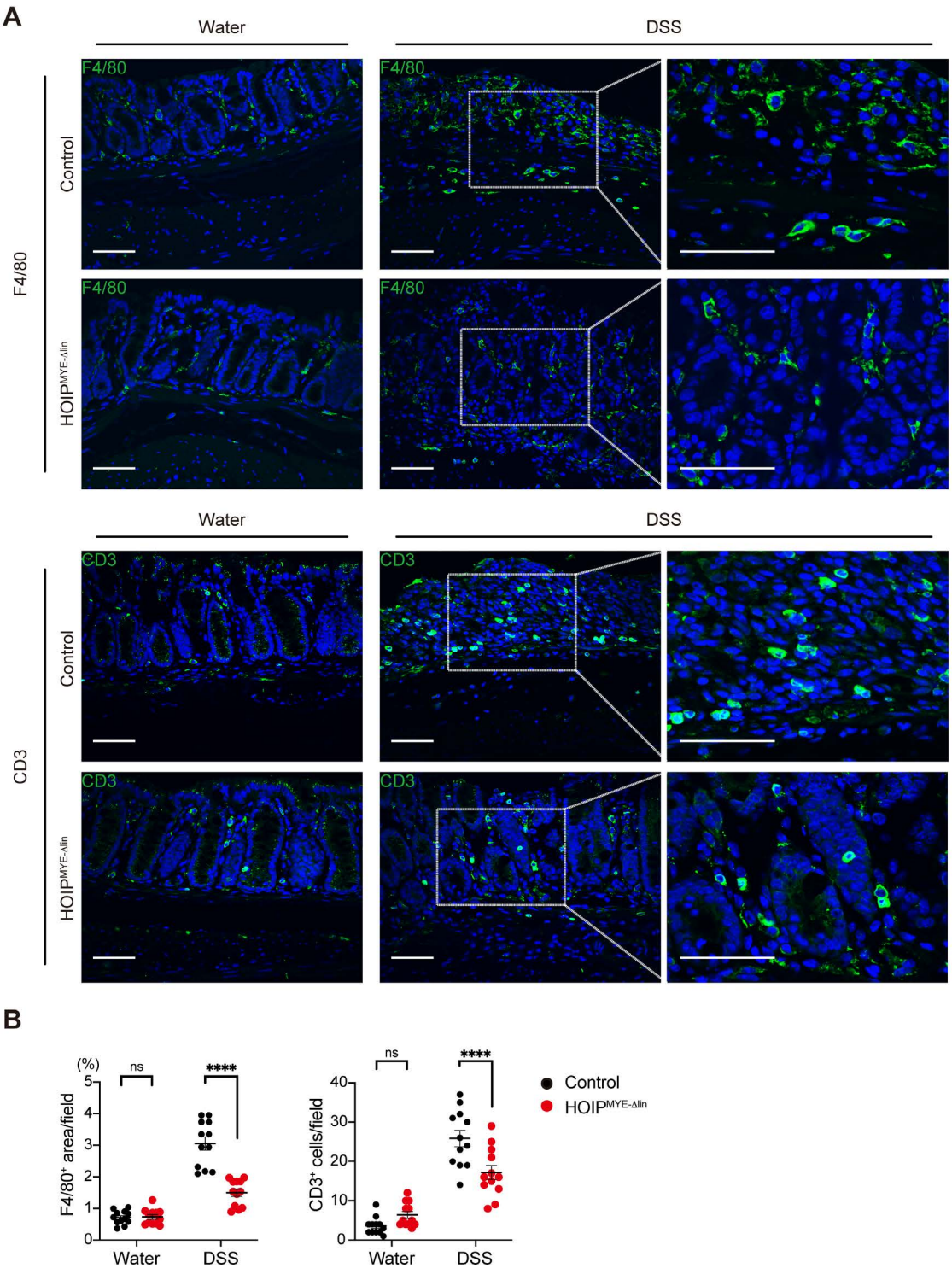

Figure S7

Figure S7. Immunofluorescence staining of F4/80 and CD3 in distal colon sections from DSS-treated control and HOIP$^{MYE-\Delta lin}$ mice.

(A) Immunofluorescence staining for F4/80 and CD3 in distal colon sections from DSS-treated control and HOIP$^{MYE-\Delta lin}$ mice (n=3). Data from untreated control and

244 HOIP$^{MYE-\Delta lin}$ mice are also shown (n=3). Scale bars, 50 μm.

245 (B) Quantification of immune cells in (A) (n=12 fields per group).

246 Statistical significance was determined by two-way ANOVA with Bonferroni's post hoc-test

247 (B).

248

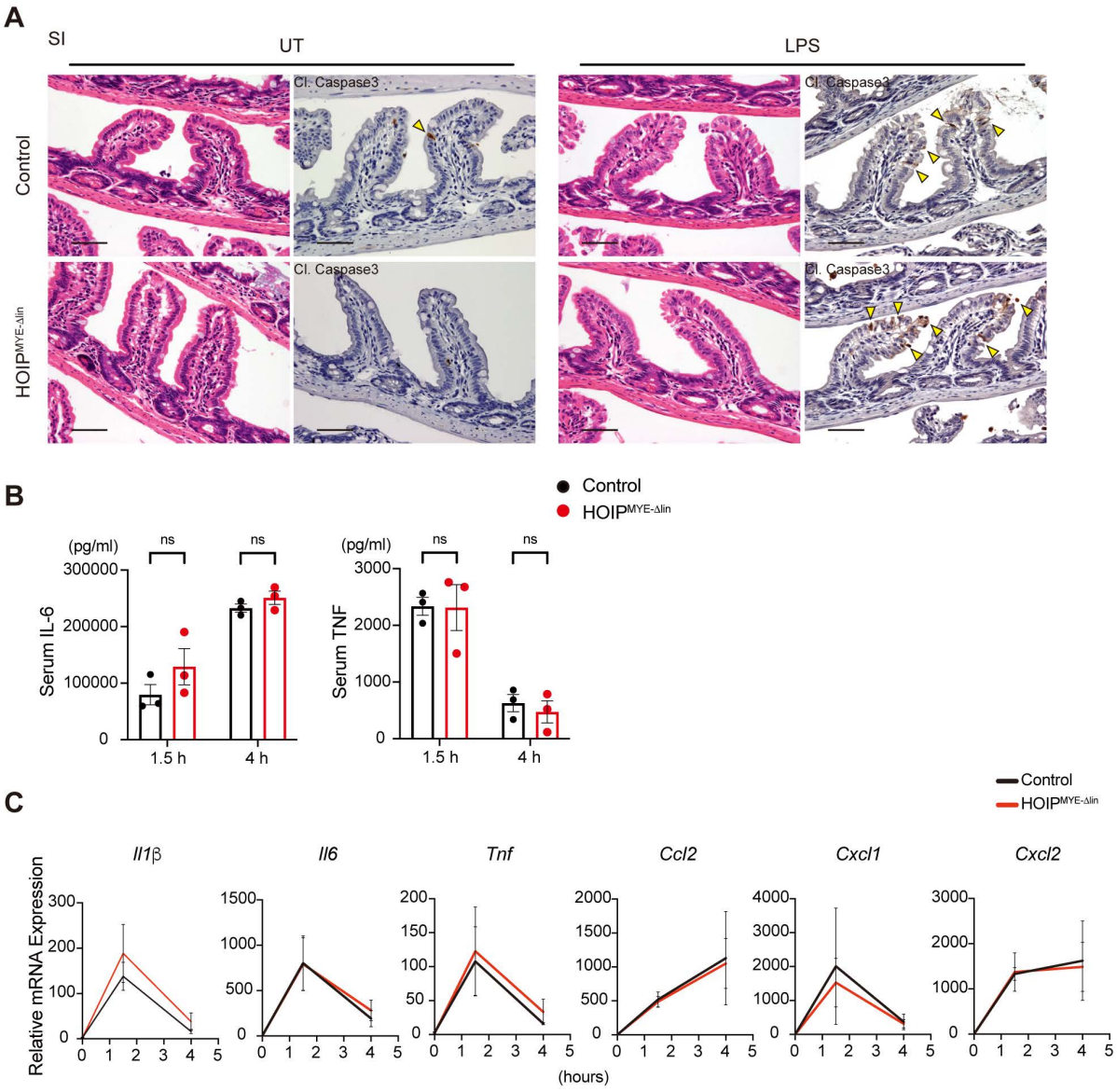

249 **Figure S8**

250 **Figure S8. Attenuation of LUBAC ligase activity in macrophages has no effect in an**

251 **LPS-induced IEC shedding model.**

252 (A) H&E staining and immunohistochemical staining of small intestine sections for cleaved

caspase 3 at 1.5 h post-intraperitoneal administration of LPS to control and HOIP$^{MYE-\Delta lin}$ mice (n=3). Data from untreated control and HOIP$^{MYE-\Delta lin}$ mice are also shown (n=3). Yellow arrows head indicate cells positive for cleaved caspase 3. Scale bars, 50 μm.

(B) ELISA used to measure serum IL-6 and TNF levels in control and HOIP$^{MYE-\Delta lin}$ mice after LPS injection (n=3).

(C) qRT-PCR analysis of inflammatory cytokine and chemokine expression in colon tissue from LPS-treated control and HOIP$^{MYE-\Delta lin}$ mice (n=3). Data are normalized to expression of *Gapdh* mRNA.

Statistical significance was determined by two-way ANOVA with Bonferroni's post-hoc test (B, C).

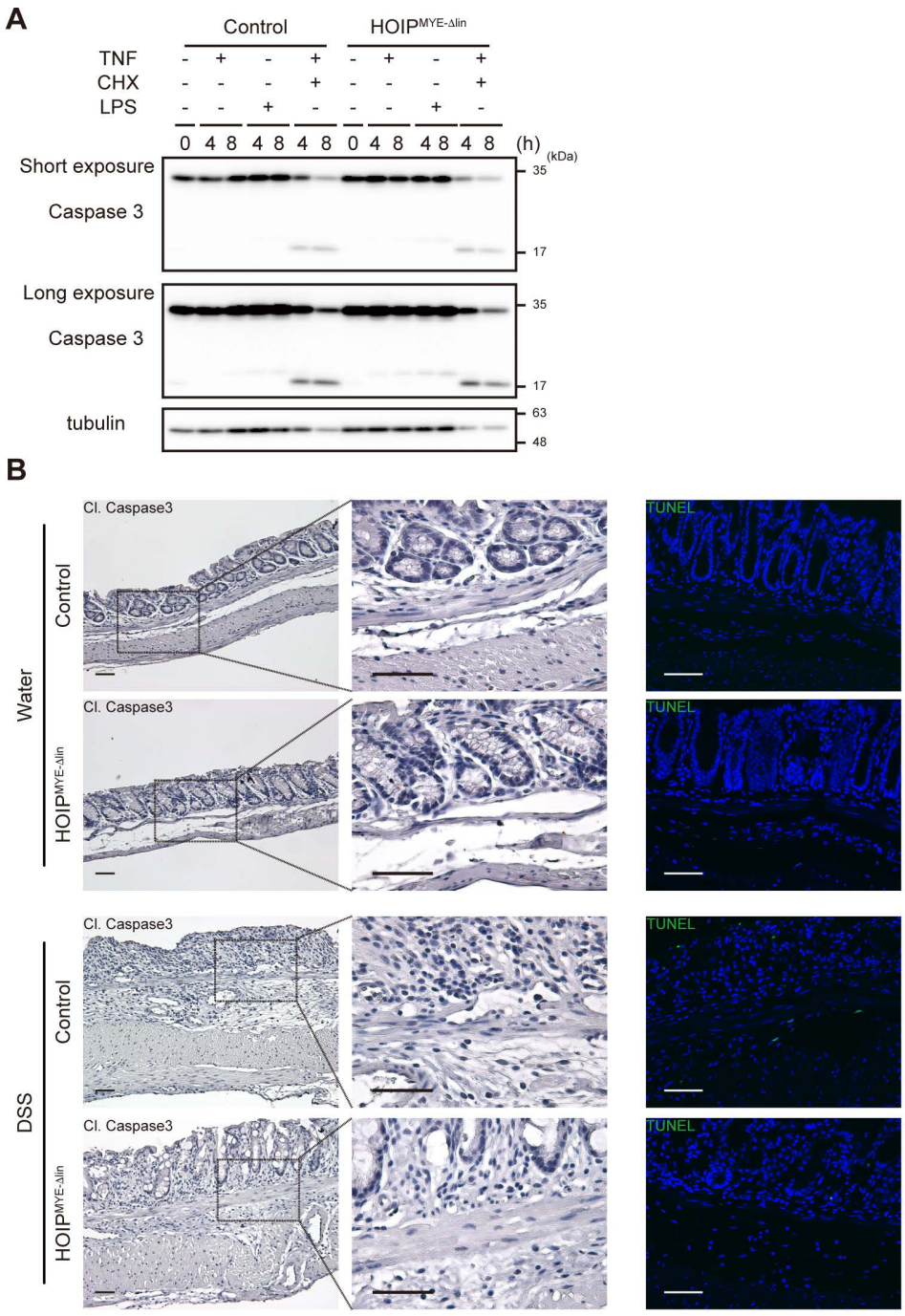

Figure S9

Figure S9. Impaired linear ubiquitination activity in macrophages has no overt effect on cell death.

(A) Immunoblot analysis of caspase 3 cleavage in BMDMs from control and HOIP$^{MYE\text{-}\Delta lin}$ mice treated with TNF (10 ng/ml), LPS (10 ng/ml), or TNF (10 ng/ml) and CHX (20 μg/ml) for the indicated periods. Tubulin was used as a loading control. Data are representative of at

least two independent experiments.

(B) Immunohistochemical staining of the distal colon sections for cleaved caspase 3, and immunofluorescence TUNEL staining, in control and HOIP$^{MYE-\Delta lin}$ mice treated with DSS (n=3). Data from untreated control and HOIP$^{MYE-\Delta lin}$ mice are also shown (n=3). Scale bars, 50 μm.

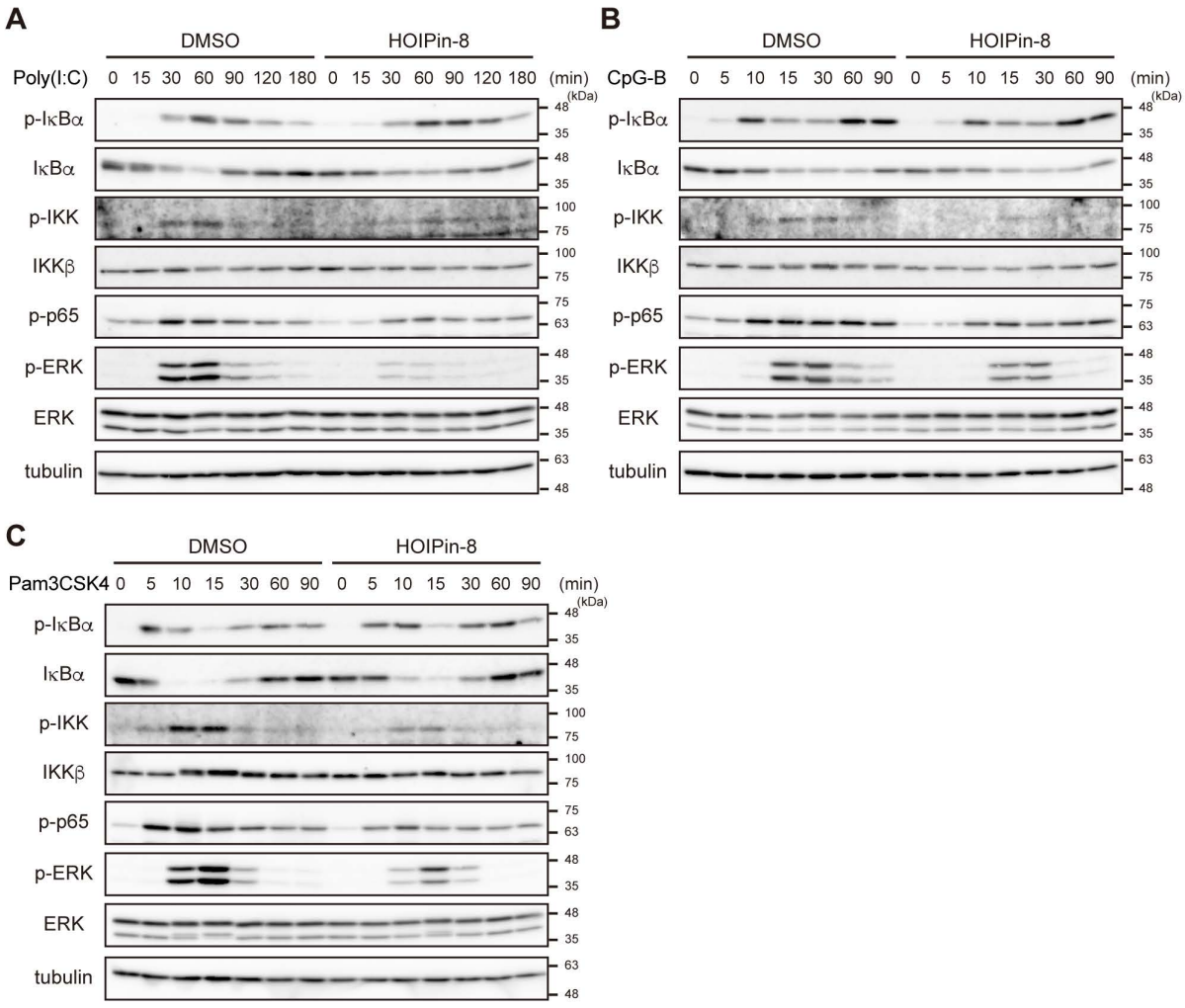

Figure S10

Figure S10. Inhibiting LUBAC ligase activity impairs NF-κB and ERK activation upon stimulation by multiple TLR ligands.

(A, B, C) BMDMs from WT mice were pre-treated for 30 min with DMSO or HOIPin-8 (10 μM) and then stimulated with Poly(I:C) (2 μg/ml) (A), CpG-B (1 μM) (B), or Pam3CSK4 (1

281 μg/ml) (C) for the indicated times. Whole cell lysates were immunoblotted with the indicated
282 antibodies. Tubulin was used as a loading control.
283 A representative image of an immunoblot from at least two independent experiments is
284 shown.
285

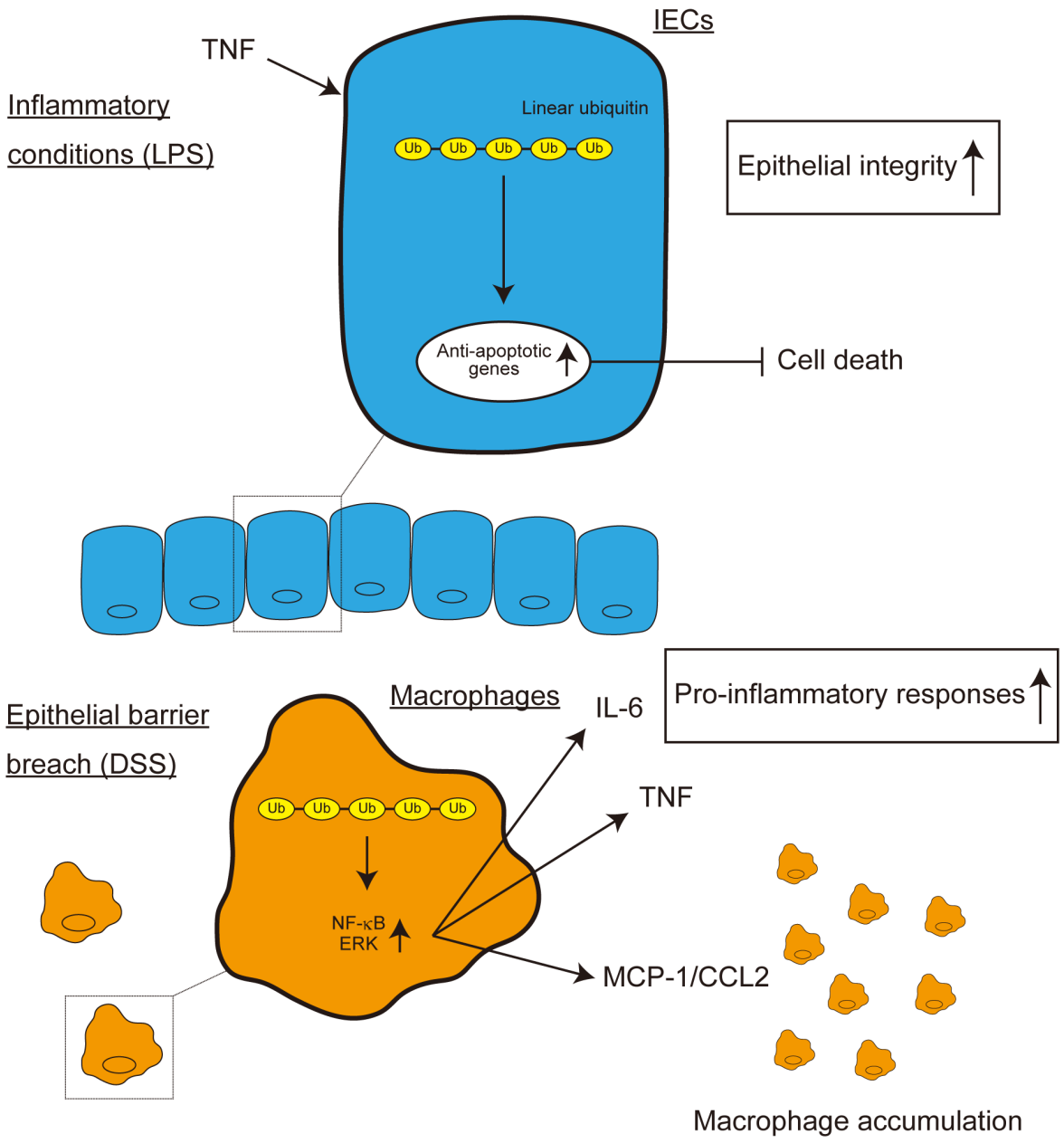

Figure S11

286

287 **Figure S11. Schematic summarizing the different functions of linear ubiquitination in**

IECs and macrophages.

Under inflammatory conditions, linear ubiquitination in IECs regulates TNF-mediated epithelial integrity by suppressing IEC death via up-regulation of anti-apoptotic genes. By contrast, in the event of an epithelial barrier breach, linear ubiquitination in macrophages regulates pro-inflammatory responses by producing pro-inflammatory cytokines (IL-6 and TNF), and a chemokine that attracts macrophages (MCP-1/CCL2) downstream of activated NF-κB and ERK.

296 **Supplementary table legends**

297 **Table S1. List of primers used for qPCR analysis**

Table S1. List of primers used for qPCR analysis

Gene		Sequence
Il1 β	Forward	5’-TGGACCTTCCAGGATGAGGACA-3’
	Reverse	5’-GTTCATCTCGGAGCCTGTAGTG-3’
Il6	Forward	5’-TACCACTTCACAAGTCGGAGGC-3’
	Reverse	5’-CTGCAAGTGCATCATCGTTGTTC-3’
Tnf	Forward	5’-GGTGCCTATGTCTCAGCCTCTT-3’
	Reverse	5’-GCCATAGAACTGATGAGAGGGAG-3’
Ccl2	Forward	5’-CCGGCTGGAGCATCCACGTGT-3’
	Reverse	5’-TGGGGTCAGCACAGACCTCTCTCT-3’
Cxcl1	Forward	5’-TCCAGAGCTTGAAGGTGTTGCC-3’
	Reverse	5’-AACCAAGGGAGCTTCAGGGTCA-3’
Cxcl2	Forward	5’-CCAACCACCAGGCTACAGG-3’
	Reverse	5’-GCGTCACACTCAAGCTCTG-3’
Birc3	Forward	5’-GGACATTAGGAGTCTTCCCACAG-3’
	Reverse	5’-GAACACGATGGATACCTCTCGG-3’
Tnfaip3	Forward	5’-AGCAAGTGCAGGAAAGCTGGCT -3’
	Reverse	5’-GCTTTCGCAGAGGCAGTAACAG -3’
Nfkbia	Forward	5’-GCCAGGAATTGCTGAGGCACTT-3’
	Reverse	5’-GTCTGCGTCAAGACTGCTACAC-3’
Lgr5	Forward	5’-CCTACTCGAAGACTTACCCAGT-3’
	Reverse	5’-GCATTGGGGTGAATGATAGCA-3’
Muc2	Forward	5’-GGTCCAGGGTCTGGA TCACA-3’
	Reverse	5’-GCTCAGCTCACTGCCA TCTG-3’
Alpi	Forward	5’-TCCTACACCTCCATTCTCTATGG-3’
	Reverse	5’-CCGCCTGCTGCTTGTAG-3’
Chga	Forward	5’-ATCCTCTCTATCCTGCGACAC-3’
	Reverse	5’-GGGCTCTGGTTCTCAAACACT-3’
Dclk1	Forward	5’-TACCGACGCTATCAAGCTGGAC-3’
	Reverse	5’-GGTAACGGAACTTCTCTGGTCC-3’
Lyz	Forward	5’-TGACATCACTGCAGCCATAC-3’
	Reverse	5’-TGGGACAGATCTCGGTTTTG-3’
Gapdh	Forward	5’-TTCACCACCATGGAGAAGGC-3’
	Reverse	5’-GGCATGGACTGTGGTCATGA-3’